buildings

MDPI

Article

Cyclic Response Characteristics of SCC Extended End-Plate Reduced Web Section (RWS) Connections

Fahad Falah Almutairi [1] and Konstantinos Daniel Tsavdaridis [2,*]

[1] Department of Civil & Architectural Engineering, College of Engineering, International University of Science and Technology in Kuwait, Al-Ardiya, Kuwait; fahad.almutairi@iuk.edu.kw
[2] Department of Engineering, School of Science & Technology, City St George's, University of London, Northampton Square, London EC1V 0HB, UK
* Correspondence: konstantinos.tsavdaridis@city.ac.uk

Abstract

This study investigates the cyclic behaviour of demountable steel–concrete composite extended end-plate reduced web section (RWS) connections for the first time, aiming to facilitate post-seismic beam replacement. A validated high-fidelity finite element (FE) model was developed to analyse 285 FE models, evaluating response characteristics based on the Ibarra–Medina–Krawinkler model. Key parameters, including the influence of composite action over the web opening, web opening diameter, and end-distance, were considered. Findings indicate that RWS connections with medium to large web openings experience cyclic strength degradation while remaining compliant with American and European seismic standards. Additionally, bolted shear studs yielded a more stable and predictable contribution to the connection's strength up to 5%, outperforming traditional welded studs in consistency. This research emphasises the importance of aligning web opening size and location with capacity design ratios between connection components for acceptable seismic performance, proposing specific web opening sizes and locations to enhance structural resilience.

Keywords: RWS connections; cyclic loading; seismic design; hysteretic behaviour; finite element analysis; bolted connections; web openings

1. Introduction

Under seismic forces, unevenly distributed yielding may impose large story drifts and high rotational demands on beam-to-column connections of moment-resisting frames (MRFs). As part of the strong connection–weak beam strategy, in RWS connections, the material is reduced from the web, and this has been proven to exhibit acceptable behaviour under such forces [1–9]. RWS connections also offer the advantage of ease in retrofitting, particularly in cases where the presence of a composite slab or beam would be highly disrupted. In such situations, only a perforation within a beam web is required, without interfering with the concrete slab.

The purpose of applying RWS connections is to control connection damage to the local yielding and local buckling of the Tee beam sections in the vicinity of the web opening, thereby generating a Vierendeel mechanism while columns remain elastic. This design approach induces additional rotation at the joint, subsequently increasing ductility and promoting local deformation in the reduced beam section [1–9]. Recent laboratory tests on demountable composite RWS connections have demonstrated the formation of the

Academic Editor: Xavier Romão

Received: 11 January 2026
Revised: 4 February 2026
Accepted: 10 February 2026
Published: 4 March 2026

Vierendeel mechanism, even when the perforation was located in a high shear zone [8]. The efficiency of this ductile mechanism relies on both the size and location of the web opening to leverage the full benefit, while also adhering to the strong column–weak beam concept [1–9].

The initial concept of using RWS connections as ductile fuses is derived from beams with single or multiple openings (aka cellular beams). SCI-P355 guidance [10] provides the main failure modes of perforated composite beams and their associated design equations. The guidance presented in SCI-P355 [10] is derived from the T-section approach (TSA), which was introduced for composite perforated beams. This approach can also be utilised to determine the capacities of non-composite perforated beams, essentially by disregarding the contribution of the RC slab. Figure 1 summarises the associated failure modes of a single web opening, which are also applicable to RWS connections. The three main failure modes of concern for RWS connections are bending of the beam at the opening, shear of the beam at the opening, and Vierendeel bending.

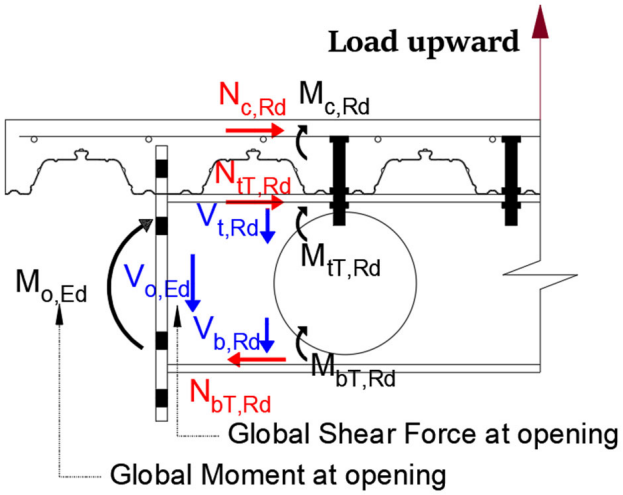

The main failure modes of single web opening - RWS connections

Bending of beam at opening	Shear of beam at opening	Vierendeel bending
$M_{o,Rd}$	$V_{o,Rd}$	$M_{v,Rd}$
$M_{o,Rd} = N_{bT,Rd}\, h_{eff} + N_{c,Rd}\, h_c$ (1)	$V_{o,Rd} = V_{bT,Rd} + V_{tT,Rd} + V_{c,Rd}$ (2)	$M_{v,Rd} = 2M_{bT,Rd} + 2M_{tT,Rd} + M_{c,Rd}$ (3)

$N_{bT,Rd}$	The tensile resistance of the bottom Tee.
h_{eff}	The effective depth of the beam between the centroids of the Tees.
$N_{c,Rd}$	The compression resistance of the concrete slab.
h_c	The slab depth.
$V_{bT,Rd}$, $V_{tT,Rd}$	The shear resistance of the bottom/top Tee.
$V_{c,Rd}$	The shear resistance of the concrete slab at the opening.
$M_{bT,Rd}$, $M_{tT,Rd}$	The bending resistance of the bottom/top Tee.
$M_{c,Rd}$	The bending resistance due to composite action of the top Tee with the slab.

All are according to the SCI-P355 guidance.

Figure 1. Main failure modes of single web opening—RWS connections.

The associated design equations for the three failure modes of RWS connections that are presented in Figure 1 were developed for monotonic loads and need to be checked for cyclic loads. The study conducted by Tsavdaridis et al. [11] shows that the cyclic moment and rotational capacities of the RWS connections were lower than their monotonic counterparts. Moreover, a recent experimental investigation on demountable composite RWS connections [8] demonstrates that the bending moment $M_{o,Rd}$ of composite RWS connections could be designed in accordance with SCI-P355 guidance [10] with acceptable overstrength factors. The Vierendeel bending capacity $M_{v,Rd}$ was overestimated in the study by Almutairi et al. [8] using SCI-P355 guidance [10]. It is worth noting that all tested RWS connections in the study [8] had a diameter of web opening (d_o) equal to 80% of the beam section's depth (h) near the connections in the high shear zone. Regardless of this, the cross-sectional shear failure due to global shear was transformed to the Vierendeel mechanism, which governed the failure of all tested RWS connections [8]. This algins with previous findings [5–7] indicating the shear forces induced by critical cross-section plastification can be transferred in a stable manner through compression and tension struts that develop in the vicinity of the openings, thereby ensuring structural integrity and reliability under cyclic loading conditions. This stable behaviour depends on the location and size of openings, along with the capacity design ratio between the components of the joint [7,8]. Thus, it is possible to infer that both the Vierendeel mechanism and limited plastification of the reduced cross-section may occur as deformation demands are imposed. For design purposes, it is efficient to establish a benchmark for moment capacity in terms of the plastification of the reduced cross-section, aiming at streamlining the design process for practitioners by eliminating the necessity to compute yielding moments associated with the Vierendeel mechanism. By adopting this methodology, capacity design actions can be readily computed, taking into account the yielding behaviour of the reduced cross-section as defined in SCI-P355 guidance [10].

The complex hysteresis behaviour of bolted extended end-plate RWS connections is a result of multiple deformable components, making their prediction challenging. Therefore, the finite element (FE) models were initially validated against a test campaign in the literature [8]. Parametric FE analyses were then performed, aiming at investigating the local cyclic behaviour of demountable steel–concrete composite RWS connections, focusing on load-carrying capacity, strength, stiffness degradation, ductility, and energy dissipation capacity. The selected parameters align with previous studies [7,8] and include (i) the presence and absence of composite action over the web opening, (ii) the diameter of web opening (d_o) and (iii) the end-distance from connection face to of web opening centreline (S_o). This study maintains a constant beam size, aiming at isolating the specific effects of such parameters on key performance characteristics of RWS connections. This focus aligns with established knowledge within the field of RWS connection behaviours [4,5,7–9]. Boushehri et al. [4] investigated several parameters including various beam sizes and concluded that the response of RWS connections is primarily governed by the size and location of the web opening, with beam size having a less significant influence. These parameters align with the test and numerical studies conducted as part of the project, aiming to non-dimensionalise all results of RWS connections and develop large databases that can then be employed for developing design guidelines for RWS connections in accordance with the European Standards.

Behaviour of Reduced Web Section (RWS) Connections—Vierendeel Mechanism

The web opening near the connection is intentionally introduced as part of the RWS design strategy rather than for utility or construction requirements. Its primary role is to relocate plastic hinge formation away from the column face toward the perforated beam

region, thereby shielding the connection and column from excessive inelastic deformation. This controlled yielding mechanism enhances ductility and seismic resilience while facilitating post-event repair or beam replacement. This intentional relocation of the plastic zone gives rise to what is commonly known as the Vierendeel mechanism.

The Vierendeel mechanism refers to the local bending action that develops around the web opening when the beam is subjected to global forces. Instead of transferring forces purely through shear, the T-sections above and below the opening behave like short beam segments that bend and form plastic hinges at the opening corners, as illustrated in Figure 2. While this mechanism reduces the elastic stiffness compared to a solid web, it significantly increases the connection's rotational capacity and energy dissipation. In practice, this behaviour often governs the connection's ultimate performance, providing a "structural fuse" before the rest of the beam reaches its limit.

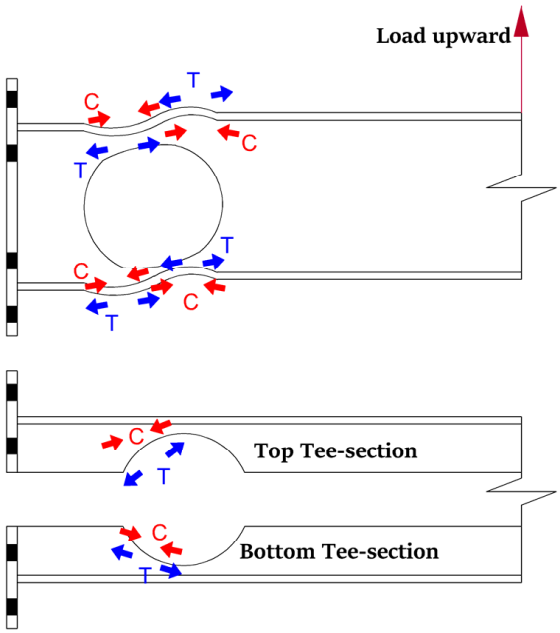

Figure 2. Vierendeel mechanism.

In RWS and other perforated steel beams, this mechanism is considered a stable and highly ductile yield response by redistributing global actions away from brittle joint components. However, the performance is sensitive to geometry; the size and location of the web opening determine whether the response remains ductile or transitions toward undesirable failure modes, such as local tearing or out-of-plane buckling. Therefore, precise detailing of the opening is essential to ensure predictable seismic performance.

2. Finite Element Model Validation

2.1. Numerical Modelling

The accuracy of the FE models was confirmed by validating the findings of a recent experimental investigation conducted on four composite RWS connections in terms of sizes and material strength [8] (Table 1 and Figure 3). The geometrical and cross-sectional details of the four tested specimens were reported by Almutairi et al. [8]. The boundary and loading conditions, including the gravity load, preloading forces and AISC 341 [12] loading protocol, were employed in FE models to simulate the ones in the experimental tests. A cantilever configuration with a strong, stocky column was adopted, and the back, top, and bottom of the column were fixed, resulting in negligible panel zone deformation so that the cyclic response was dominated by the RWS and connection region. The distribution of residual stresses, obtained from testing the solid specimen, was applied to the validated

FE model of RWS-L-retrofit in order to simulate the effects of moderate seismicity for rehabilitation purposes [8]. An imperfection was initially applied by selecting the first shape of Eigenmode (Figure 3) and scaled by the recommended factor of $t_w/200$ in accordance with [13]. It is worth mentioning that the solid specimen was cyclically loaded only up to approximately 70% of its positive (sagging) moment capacity, rather than to full plastic failure, to represent the effects of moderate seismic events over time. Subsequently, a web opening was introduced, and the specimen (RWS-L-retrofit) was subsequently re-tested.

Table 1. Specimen test matrix [8].

Specimen ID		Solid Specimen	RWS-L-Retrofit *	RWS-L	RWS-H
Connection Type		Extended end-plate	EEP RWS		
Composite action			Low (L)		High (H)
Web opening (mm)	Diameter d_o	-	0.8h	0.8h	0.8h
	End-distance S_o		1h	0.8h	0.8h
S_e (mm)			600		300
Connection Category		Partial strength	Full strength		

Note: * A web opening was created into the solid specimen and then retested for rehabilitation purposes. L, H, h, 80h, and 80S = are defined in Table 2. S_e = the distance between the centreline of the first shear stud row and the connection face. S_o = the distance between the centreline of web opening to the connection face.

Table 2. Parameters.

* (1) Diameter d_o			** (2) End-Distance S_o		(3) The Presence of Composite Action over the Web Opening (3 Categories)
%	mm	No. of Models	%	mm	
50%	155	15	50%	155	Yes—High composite action
55%	171	14	55%	171	No—Low composite action
60%	186	13	60%	186	Bare steel connection (Non)
65%	202	12	65%	202	
70%	217	11	70%	217	
72% ***	223	11	72% ***	223	
75%	233	10	75%	233	
80%	248	9	80%	248	
Total 95			85%	264	
Number of models in each set of diameter × 3 Categories (1—High, 2—Low and 3—Without composite slab) **Total parametric models = 3 × 95 = 285**			90%	279	
			95%	295	
			100%	310	
			105%	326	
			110%	341	
			115%	357	
			120%	372	

Note: Low (L) and High (H) composite action = where the studs are avoided and placed over the web opening, respectively. h = beam height; 80d_o = web opening diameter is equal to 80% of h; 80S_o = the end-distance is equal to 80% of h. * FE models with d_o = 50% start with S_o = 50%, FE models with d_o = 55% start with S_o = 55%, and so on. ** All models were compiled to SCI-P355 [10] in terms of the width of the end-post. *** Maximum web opening diameter considering the depth of Tee section limitation in accordance with SCI-P355. Therefore, d_o = 75% and 80% are beyond SCI-P355.

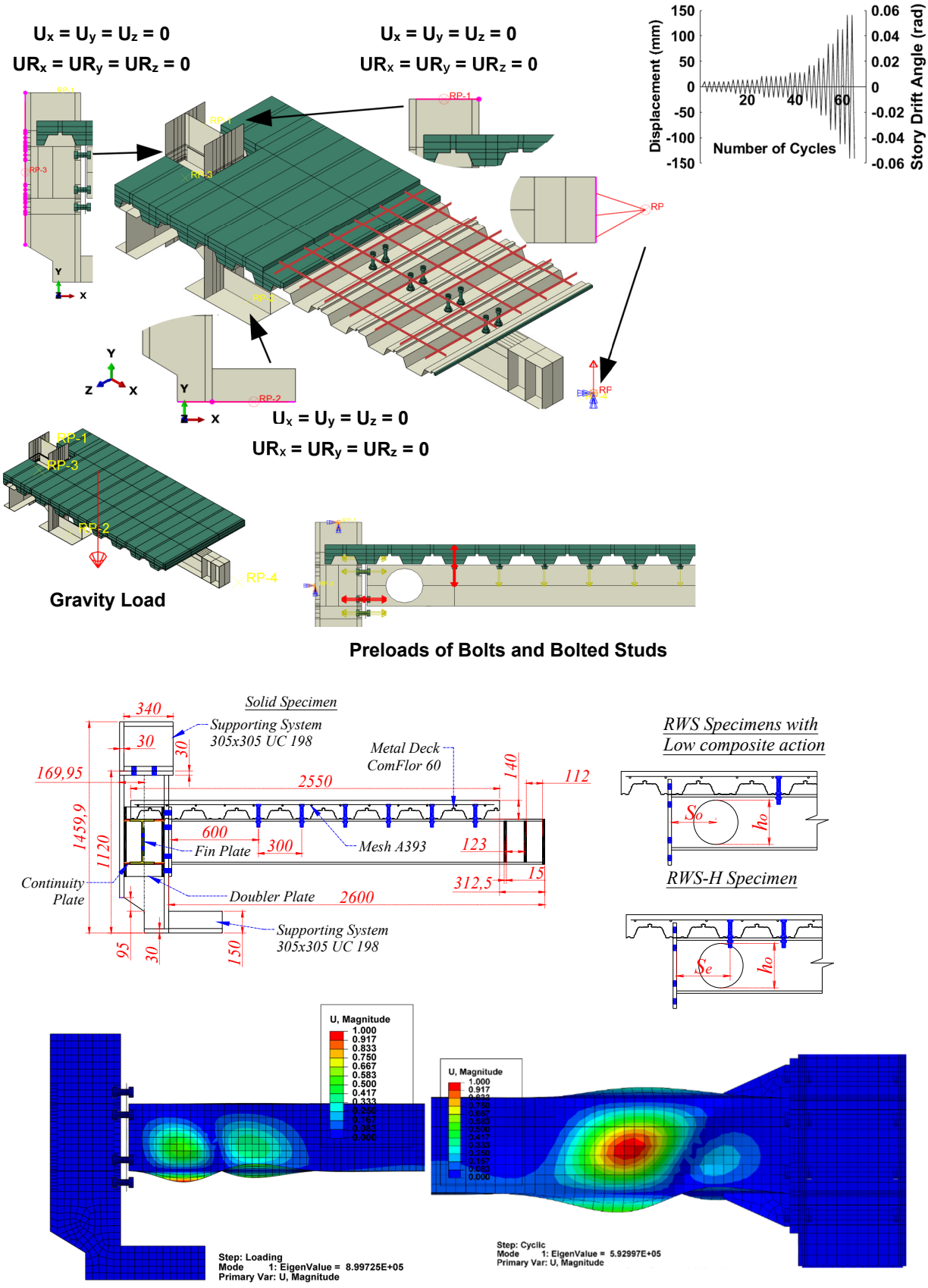

Figure 3. 3D test set-up (mm) [8], cyclic loading protocol and first shape of eigenmode.

The composite metal deck slab, bolts, and bolted shear studs were modelled with 8-node solid elements with reduced integration (element type C3D8R). All other elements were modelled with 4-node shell elements with reduced integration (S4R) including the

metal deck, as shown in Figure 3. The reinforcement steel bars were modelled using truss element (2-node linear, T3D2), which can carry only tensile and compression loads and exclude any resistance to bending. Tie constraints were applied to simulate the welding between steel elements. Normal and tangent interactions were employed between steel-to-steel elements by defining hard contact and formulation of a friction coefficient equal to 0.2 (which corresponds to the case of untreated rolled surfaces [14]) and with a finite sliding approach. Tie contact was considered between the reinforced concrete component and metal deck of the composite slab to avoid numerical instabilities in some parametric FE models, which can lead to early termination of the analysis. Also, this modelling technique was adopted to decrease the computational time in parametric FE models.

2.2. Material Model

Material non-linearities were adopted by employing a combined isotropic and kinematic material-hardening (half cycle) model from ABAQUS 2019 [15] for all steels. This combined model (half cycle) offers a more accurate representation of the stress–strain response compared to the linear kinematic model. It defines the yield surface size as a function of equivalent plastic strain and incorporates other cyclic loading phenomena like stress relaxation, ratcheting, and cyclic hardening [15,16]. According to the ABAQUS manual [15], the combined model (half cycle) is utilised if limited test data are available (e.g., cyclic steel material testing), since the mathematical operation in ABAQUS will determine a kinematic hardening modulus (C) and a rate (γ) at which the kinematic hardening modulus decreases with increasing plastic deformation [15]. Material tri-linear and bi-linear stress–strain curves in Almutairi et al. [7] and Almutairi and Tsavdaridis [17] are adopted for (i) all steel elements, including bolts and bolted shear studs, and (ii) metal deck and steel reinforcement, respectively. The average values of tensile tests for beam web and flange were considered, and nominal values of materials properties were taken from the manufacturer's specifications [8]. The ultimate strain (ε_u) was equal to $15\varepsilon_y$ for all steel elements and $10\varepsilon_y$ for bolts and bolted shear studs. ε_r was set to 0.2 for all steel elements and to 0.05 for the bolts and bolted shear studs. The ductile damage option was used to consider the effect of the cracks that occurred in the vicinity of the web opening during the experimental tests [8]. The values of ductile damage were extracted as described in the ABAQUS manual [15], from the tensile tests of beam web that were conducted in the literature [8].

The concrete damaged plasticity (CDP) model was employed for modelling the inelastic behaviour of concrete. The concrete behaviour in compression was defined based on the constitutive law of EC2 [18], while the concrete behaviour in tension was defined based on the exponential tension softening of Cornelissen et al. [19], as shown in Figure 4. The average value of three compression cylinder tests of concrete was used with the axial tensile strength f_t taken as 10% of the compressive strength of f_{ck} 31.28 MPa [20]. The other five plasticity parameters for CDP, namely the dilatation angle (=30°), eccentricity (=0.1), the ratio of bi-axial-to-uniaxial compressive strength (f_{b0}/f_{c0} = 1.16), the K parameter (=0.6667), and viscosity (=0.0005), were assumed as the default values given in ABAQUS. More details of the concrete behaviour in compression and tension are available in Ahmed and Tsavdaridis [21], Almutairi et al. [7], and Almutairi and Tsavdaridis [17].

A mesh sensitivity analysis was performed using various mesh sizes to assess the time, storage, and accuracy of the results. As shown in Figure 5, Models 1, 2, and 3 used uniform mesh sizes of 10 mm, 20 mm, and 30 mm, respectively, for the steel components and slab, while a consistent mesh size of 7.5 mm was applied to the bolts and bolted shear studs across all three models. Model 1, being the most refined, resulted in over 430,000 elements and 480,000 nodes, while Model 3 had significantly fewer—approximately

44,000 elements and 56,000 nodes. In contrast, the adopted model utilised a hybrid meshing strategy to optimise the trade-off between result accuracy, analysis time, and memory usage. Specifically, mesh sizes of 30 mm, 50 mm, and 7.5 mm were used for the steel components, slab, and bolted details, respectively, with a refined 20 mm mesh applied to a 600 mm region near the connection, where high stresses and strains were expected. The total number of elements was 35,551. These FE modelling techniques were defined to best simulate the hysteretic behaviour of the experimental tests [8] and to limit the analysis running time between 11 to 15 h (i.e., one session on the High-Performance Computer). The FE analyses were terminated at a target drift ratio of 0.04–0.05 rad to ensure consistency and computational control rather than due to numerical instability or global structural collapse. The reported strength degradation was therefore evaluated within this predefined deformation limit.

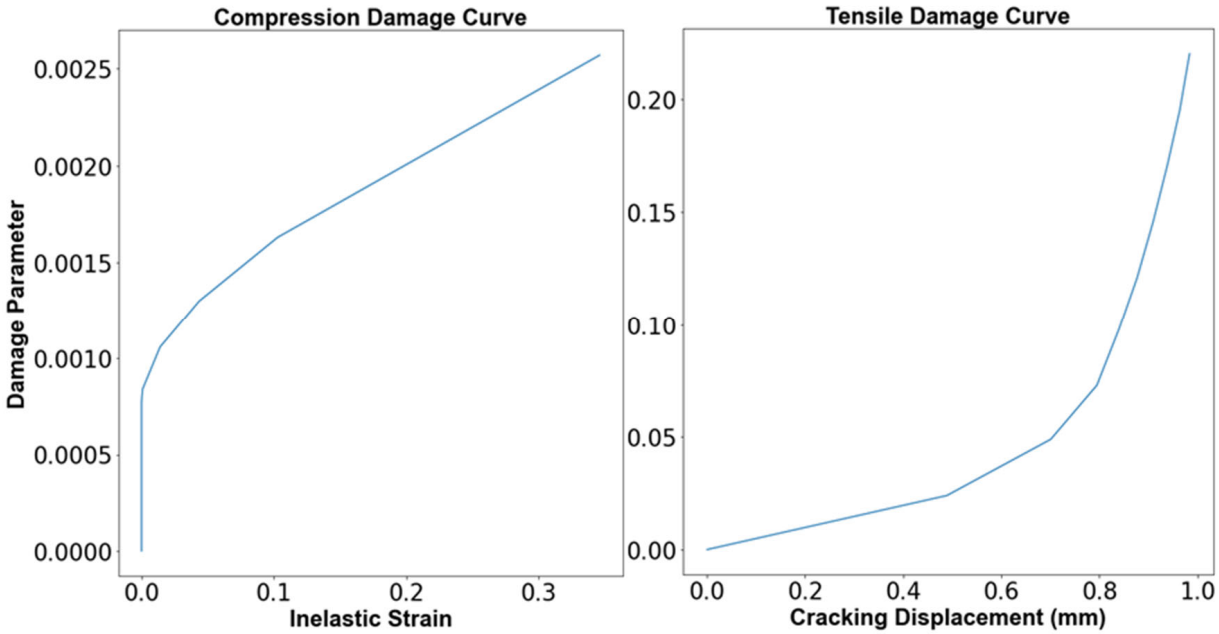

Figure 4. Compression and tensile damage curves.

2.3. FE Verification

FE models were validated against experimental test results [8] to ensure accurate representation of structural response. Figure 6 compares the moment–rotation relationships at the column face for four different connection configurations: Solid-L, RWS-L-retrofit, RWS-L, and RWS-H. For each specimen, both the positive (sagging) and negative (hogging) moment capacities obtained from the FE simulations are compared to those from physical testing.

The FE results demonstrated good agreement with the experimental curves in terms of initial stiffness, yielding behaviour, and post-yield softening. The deviations in peak moment capacities were quantified in both directions. In the sagging direction, the difference between FE and test results ranged from +3% to +6%, while in the hogging direction, the difference ranged from −2% to −5%, as annotated in Figure 6. These differences are within acceptable bounds and confirm the accuracy of the modelling assumptions.

Overall, the FE models effectively captured the nonlinear cyclic behaviour of the tested connections. The close match in peak values and curve shape indicates the models are sufficiently robust for use in parametric studies and further sensitivity analyses.

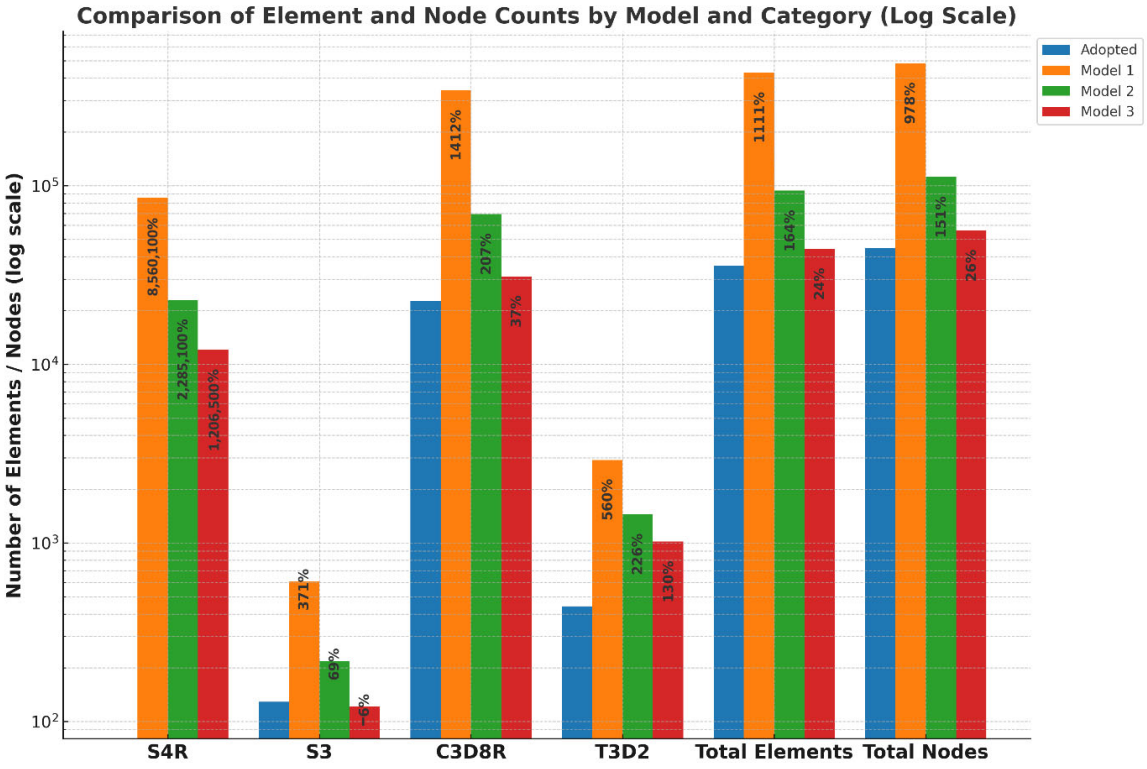

Figure 5. Comparison of element and node counts by model and category (log scale).

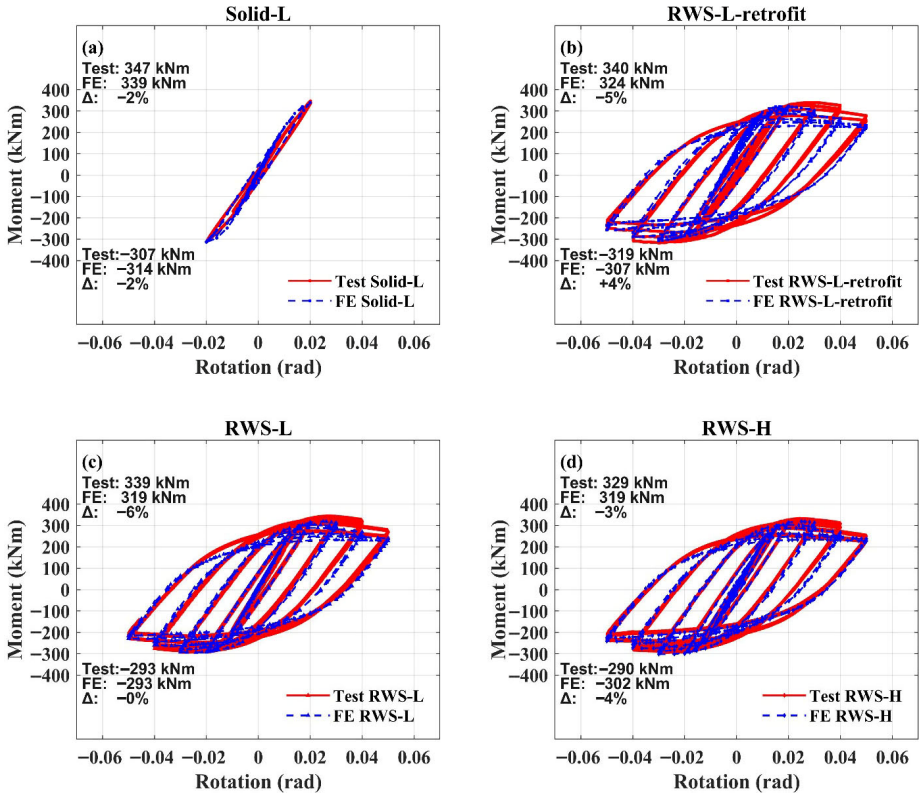

Figure 6. Comparison between experimental and FE moment–rotation responses.

2.4. Failure Mode Comparison

The FE models were further verified by comparing the predicted failure patterns to those observed in the physical tests. Figure 7 illustrates side-by-side visual comparisons for all key specimens.

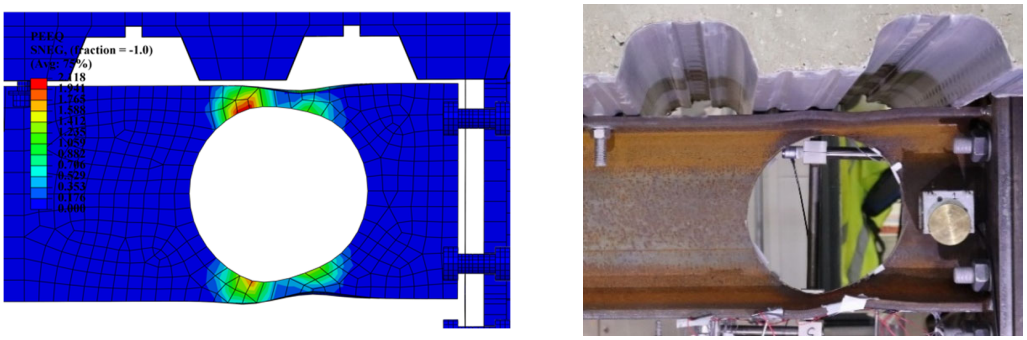

(**a**) Comparison between FE model and tested RWS–L specimen (shell thickness is not shown).

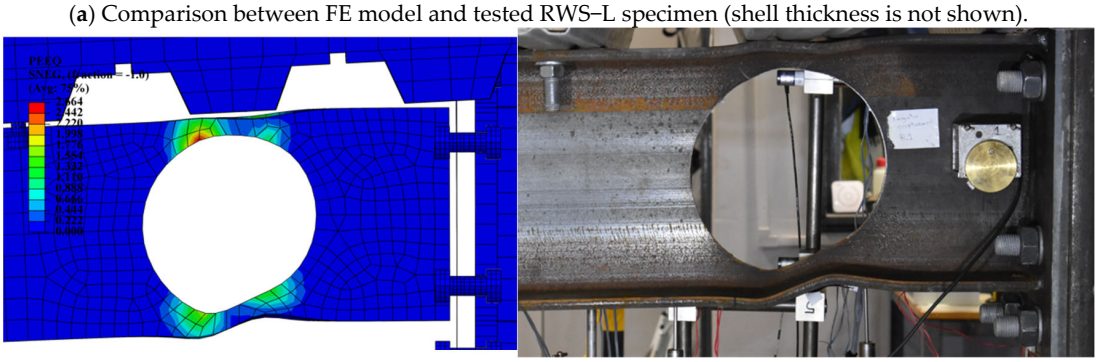

(**b**) Comparison between FE model and tested RWS-L–retrofit specimen (shell thickness is not shown).

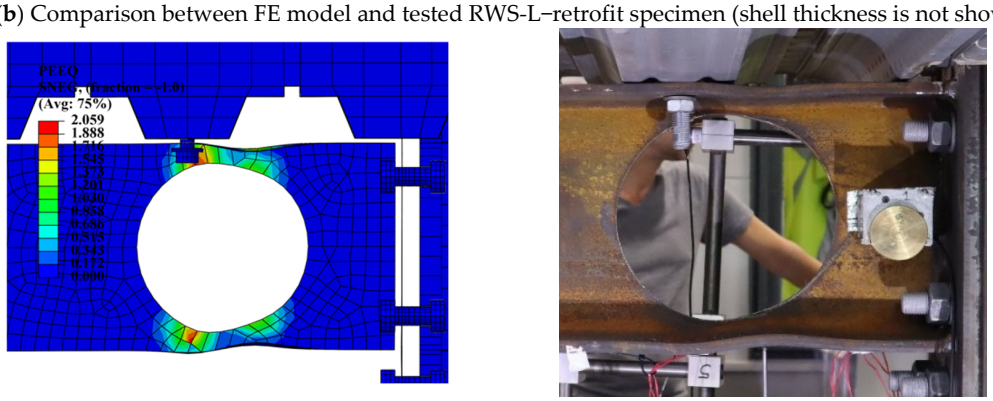

(**c**) Failures of RWS–H

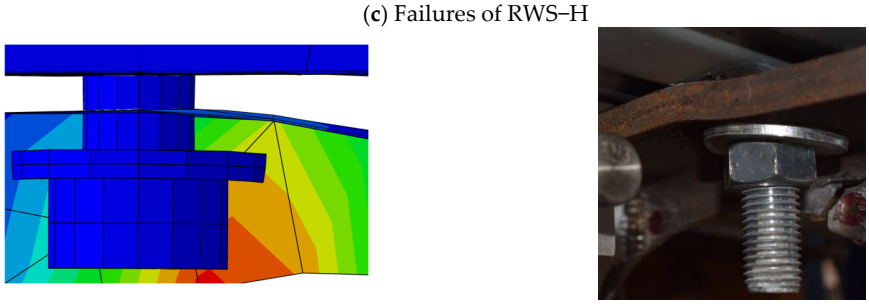

(**d**) Bending of bolted shear studs in RWS–H specimen after testing.

Figure 7. Comparison between FE models and tested specimens (shell thickness is not shown).

In Figure 7a, the FE model of the RWS-L specimen shows localised plastic deformation concentrated around the web opening, particularly at the upper and lower edges—a pattern consistent with the experimental test, where visible distortion and yielding occurred in the same regions. The FE simulation accurately captured the stress concentration zones adjacent to the hole.

Similarly, in Figure 7b, the RWS-L-retrofit specimen exhibited comparable deformation patterns in both the FE model and the tested specimen. The RWS-L-retrofit specimen was modified from a solid-web beam by introducing a web opening as a retrofit strategy after moderate seismic activity. The FE model effectively reproduced the result-

ing deformation patterns, confirming the FE model's ability to represent the improved performance effectively.

Figure 7c presents the RWS-H specimen, which developed higher levels of localised strain and deformation in the web opening region, particularly in the diagonal shear bands near the hole corners. Figure 7c confirms this with pronounced visible deformation and material thinning in the same regions. The FE model captured this progressive web failure behaviour, demonstrating a reliable representation of the physical mechanism.

Finally, Figure 7d focuses on the failure of the bolted shear studs in the RWS-H configuration. The FE model successfully predicted the bending and distortion of the studs under combined shear and axial demands, which was confirmed by the post-test photo showing significant shear stud bending.

These observations confirm that the FE models not only captured the global cyclic response but also accurately predicted local failure mechanisms, including yielding near the web opening and bolt group deformation, providing confidence in their use for further parametric investigation.

3. Parametric Investigation

3.1. Parameters

Following the FE modelling validations, a total of 285 parametric FE models were developed for RWS connections with various configurations, as shown in Table 2. Three additional FE models of solid-webbed connections (without web openings) were developed for comparison. Table 2 presents the three parameters selected to investigate the effect of the presence of composite action to the plastic zone (i.e., web opening) on the performance of a steel–concrete composite bolted extended end-plate RWS connection subjected to cyclic loading. This study aims to address the extant knowledge gap regarding the cyclic response characteristics of RWS connections with composite slabs by comprehensively analysing the findings of parametric investigation to promote the use of RWS connections in MRFs in seismic areas.

In this study, the end-distance, S_o, complies with SCI-P355 [10], which specifies the minimum width of the end-post, from the column face to the edge of the web opening. Accordingly, the FE models with a web opening diameter d_o of 50% of the beam's depth (h) start with an end-distance S_o equal to 50% of h to comply with SCI-P355 [10]. Similarly, for FE models with $d_o = 0.55h$, start with S_o equal to $0.55h$. This guide applies to all different diameters considered in the study. The presence and absence of bolted shear studs above the web opening was used to classify the specimens as having high (H) or low (L) composite action, respectively, according to EC8-1 clause 7.7.5 and ANSI/AISC 358-16 [22,23]. The steel elements and concrete slab were kept the same as in the experimental test [8] in terms of dimensions and material grades.

The selected parameter ranges were intentionally defined to reflect commonly adopted beam–column node configurations in steel and composite MRF practice, as reported in design guidance (SCI-P355, EC3/EC8, ANSI/AISC 358) [10,22,23] and previous experimental studies [4,8,9]. By maintaining constant beam size and material grades while varying only the dominant geometric and composite variables, the parametric set ensures both physical representativeness and generalisability of the results to typical engineering applications.

3.2. Connection Response Characteristics

This section evaluates the characteristics of the cyclic response of RWS connections based on the deduced response parameters of interest, such as stiffness, moment capacity, hysteretic response, ductility and the contribution of the steel–concrete composite metal deck slab. The selected cyclic response parameters (both strength and deformation) of the

Ibarra–Medina–Krawinkler (IMK) model [24] were employed in this study, as illustrated in Figure 8. The skeleton moment–rotation $(M-\theta)$ curves derived from the hysteretic curves of 285 FE models of bolted RWS connections were employed to identify the hysteresis characteristic points, as shown in Figure 9. The skeleton $(M-\theta)$ curves, taken at the column face, illustrate the hysteretic behaviour of beam web opening as one component of the extended end-plate RWS connection, to be incorporated into the component method adopted in Eurocode 3 Part 1−8 [25].

Figure 8 illustrates the stages of defining the following strength and deformation parameters of the IMK model [24]:

- The elastic (K_e) and strain-hardening stiffnesses (K_s).
- The effective yield moment (M_{ye}) and its corresponding rotation (θ_y).
  - ➢ If skeleton $M-\theta$ curves are taken at column face, M_{ye} represents the plastic moment resitstance of the connection ($M_{j,Rd}$).
  - ➢ If skeleton $M-\theta$ curves are taken at opening centreline, M_{ye} represents the bending moment resitstance at web opening centreline $(M_{o,Rd})$.
- The capping/maximum moment resistance ($M_c = M_m = M_{m,Rd}$) and its corresponding rotation (θ_m).
- The residual/ultimate/failure moment ($M_r = M_u = M_f$) and its corresponding rotation (θ_u).

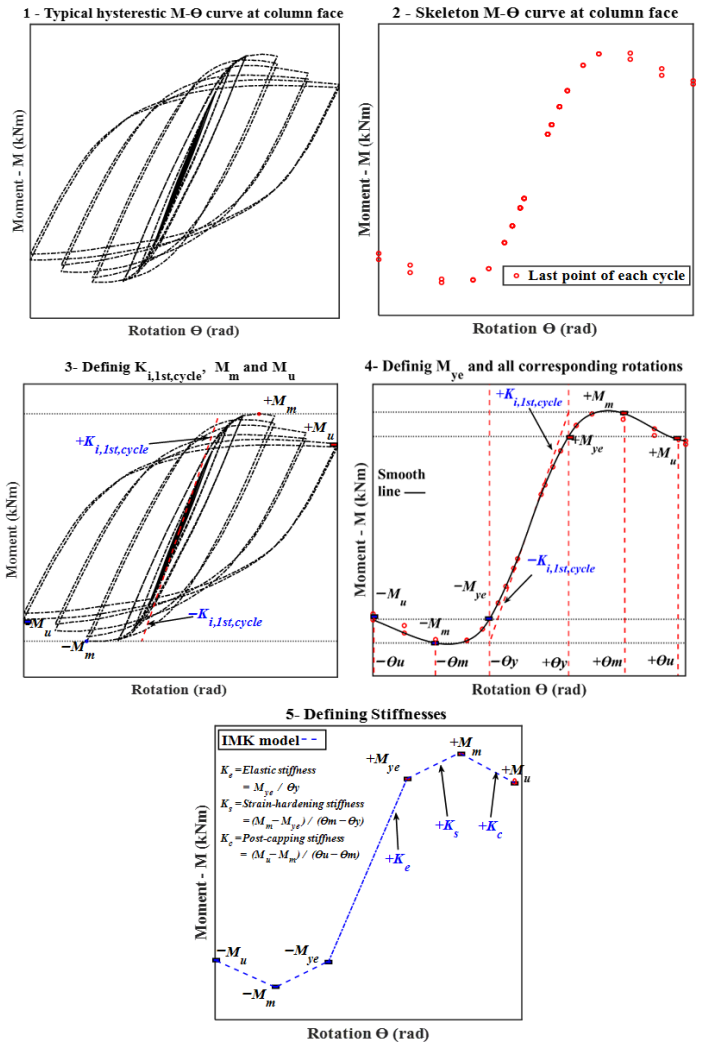

Figure 8. Deduction of characteristic points according to the Ibaraa–Medina–Krawinkler (IMK) model.

The first parameters to be defined in hysteretic curve to draw skeleton $M-\theta$ curves are initial stiffness (K_i) of hysteretic curve and the maximum moment strength $(M_{m,Rd})$. Initial stiffness (K_i) of hysteretic curve is calculated by dividing the first cycle's moment by its rotation $(K_i = M_i/\theta_i)$. Knowing K_i and $M_{m,Rd}$, the plastic moment resistance $(M_{ye} = M_{o,Rd} = M_{j,Rd})$ is defined as the point of intersection where the tangent line drawn at the point of maximum moment strength $(M_{m,Rd})$ intersects with the line representing the initial stiffness. Then, all corresponding rotations (i.e., θ_y and θ_m) can be defined accordingly. The elastic rotational stiffness (K_e) can be defined by the yield moment by its corresponding rotation $(K_e = M_{ye}/\theta_y)$. The strain-hardening stiffness (K_s), is calculated using the following equation:

$$K_s = \frac{M_{m,Rd} - M_{ye}}{\theta_m - \theta_y}$$

In this study, the ultimate moment (M_u) represents the moment of the last cycle in cases where strength degradation occurs. If skeleton $M-\theta$ curves do not experience strength degradation, M_u would be equal the maximum moment strength $(M_{m,Rd})$. Then, all corresponding rotations can be defined accordingly.

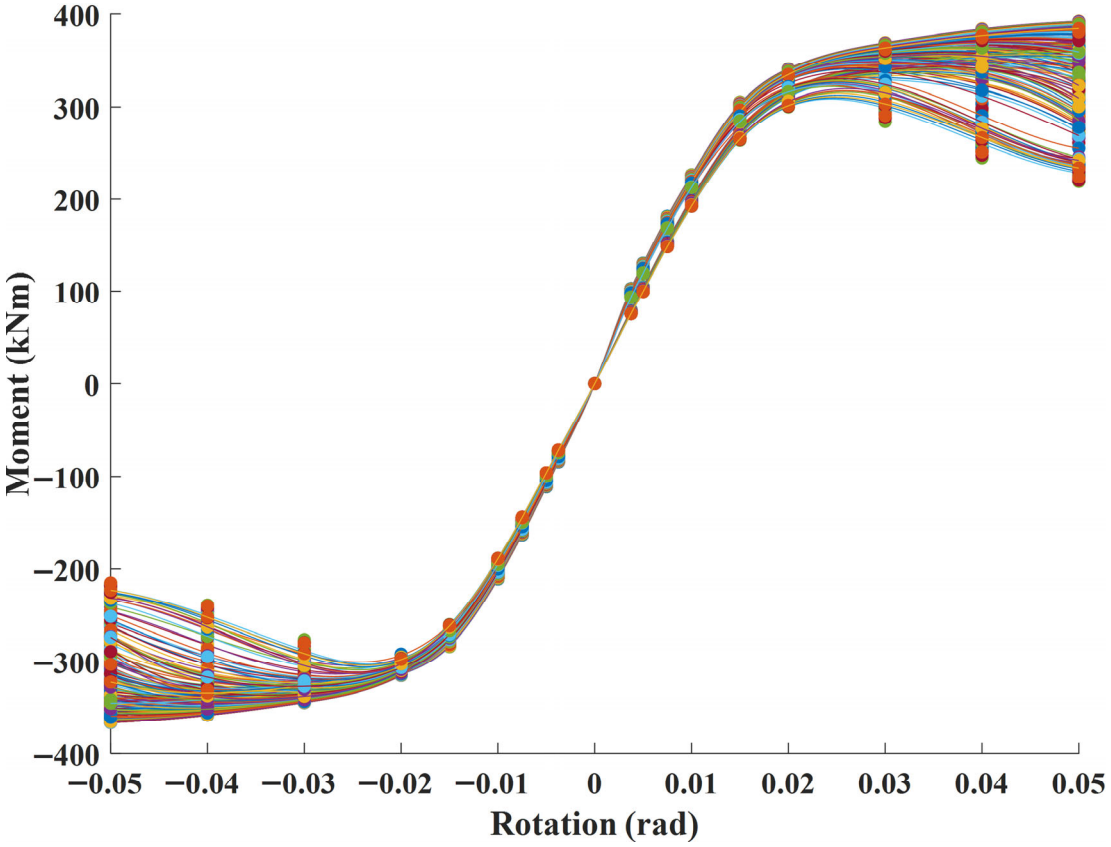

Figure 9. Skeleton moment–rotation $(M-\theta)$ curves derived from the hysteretic curves of 285.

3.2.1. Stiffness and Moment Capacity

This section explores the influence of the selected parameters on (i) the stiffness and moment capacity of RWS connections compared to those without openings, and (ii) the estimations provided by Eurocode 3 [25], highlighting potential design considerations.

Eurocode 3 classifies connections based on their stiffness and strength [25]. In unbraced frames, a connection's stiffness is classified as semi-rigid if its initial stiffness $(S_{j,ini,EC3})$ falls between $0.5\ E_b I_b/L_b$ and $k_b\ E_b I_b/L_b$, where k_b is equal to 25 for MRFs, E_b represents the measured steel beam elastic modulus, I_b is the beam moment of inertia about the section's

major axis, and L_b is the beam length between column centerlines. It is obvious that the component method presented in Eurocode 3 tends to overpredict the elastic stiffness (K_e) of all connections (with and without web opening), as shown in Figures 10 and 11. This observation aligns with the findings of Ding and Elkady [26]. Figures 10 and 11 confirm the semi-rigid nature of extended end-plate connections. The average differences between the initial stiffness in accordance with the Eurocode's component method ($S_{j,ini,EC3}$) and the initial stiffness of the first cycle (K_i) were about 29% and 25% under sagging and hogging, respectively. The average differences between $S_{j,ini,EC3}$ and the elastic stiffness (K_e) of all connections, based on the IMK model, were roughly 23% in both directions. Consequently, when designing RWS connections, it is recommended that appropriate adjustment factors are incorporated into the Eurocode's design method to account for the observed overestimation in stiffness.

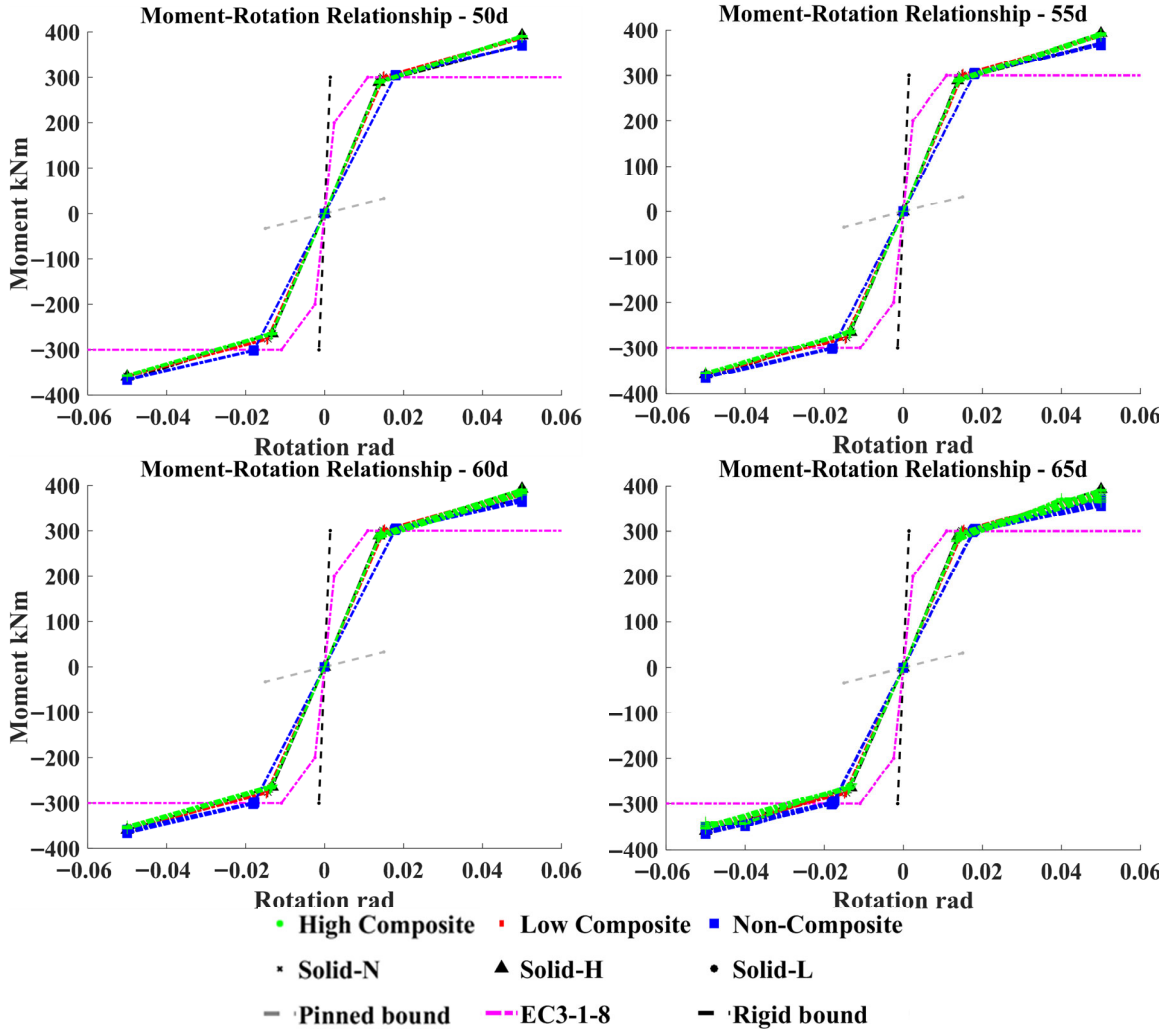

Figure 10. Skeleton curves of RWS connections with diameter = 0.5, 0.55, 0.6 and 0.65*h* (Set 1).

A quantitative assessment of the impact of the selected parameters on the stiffness of RWS connections was undertaken by comparing the elastic rotational stiffness (K_e) of RWS connections with that of connections featuring solid-webbed beams. Two sets of web openings were analysed: Set 1 with diameters equal to 50%, 55%, 60%, and 65% of the beam depth, and Set 2 with diameters of 70%, 72%, 75%, and 80% of the beam depth, as shown in Figures 10 and 11, respectively. As anticipated, the composite action—classified into Low (L), High (H), and Non-composite (N) based on the placement of studs—further influences the connection's stiffness. High composite action, where studs are placed over

the web openings, generally enhances the connection stiffness compared to Low and Non-composite actions by ensuring better integration between the steel beam and the concrete, thereby distributing the loads more effectively across the composite section. In comparison to the solid-webbed connections (without openings), the maximum reductions in stiffness under both directions, on average, are 7.76%, 3.16% and 20.25% for High, Low, and Non categories, respectively.

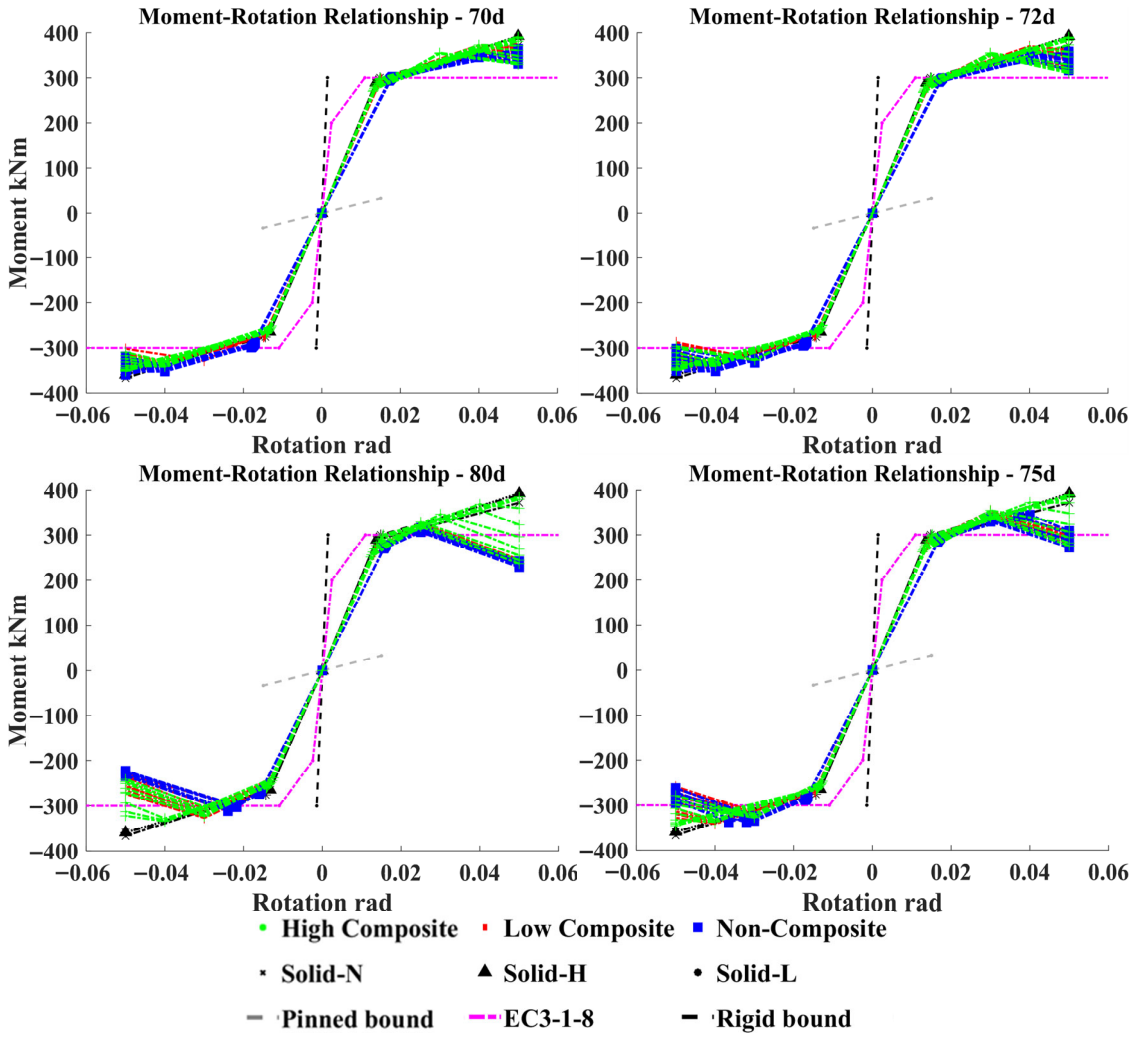

Figure 11. Skeleton curves of RWS connections with diameter = 0.7, 0.72, 0.75 and 0.8*h* (Set 2) (Solid−N means non−composite solid-webbed steel beam).

Although the skeleton curves appear similar, the presence of web openings consistently reduced stiffness across all categories (High, Low, and Non). This reduction was more pronounced for connections without a composite slab (Non) compared to those with composite action (High and Low). The stiffness of RWS connections is generally expected to decrease as the size of the web opening increases due to the reduction in the web area available to transfer shear forces and moments. Larger web openings, particularly those in Set 2, would likely exhibit a more significant reduction in stiffness compared to those in Set 1. This is because the structural integrity of the beam is compromised more as the web opening approaches 80% of the beam depth, increasing the flexibility and decreasing the beam's capacity to resist deformation under load.

Asymmetrical stiffness implicates differential structural responses under seismic loads, leading to potentially larger deformations and increased damage, particularly in structures with lower stiffness in hogging moment conditions. To address this, the data supports a

maximum opening size of 60% of the beam depth with end-distances between 65% and 90% of the beam depth for High and up to 120% for Low, to maintain a balance between structural integrity and design flexibility when stiffness is the primary concern. However, when larger web openings are used, shorter end-distances should also be applied for both High and Low. This action helps to effectively integrate the steel and concrete, distribute loads more uniformly, and enhance the overall seismic resilience of the structure.

For strength classification, the connection can be categorised as either full-strength or partial-strength based on the capacity design ratio between the connection itself and the connected steel beam. According to the European projects of EQUALJOINTS and EQUALJOINTS-Plus (EJs), the connection can be classified as equal-strength if the capacity design ratio equals 1.0 and the plastic deformations occur in both the beam and the connection [27–29]. The findings of EJs projects are adopted in the new generation of Eurocodes. In the current Eurocode 3-1-8 [25], the equal-strength connection is categorised as a partial-strength connection. In this study, the connection was designed as equal-strength [8] based on the nominal plastic bending capacity ($M_{pl,a,Rd}$), of the connected steel solid-webbed beam, without considering the composite action contribution. Thus, the incorporation of web opening alters the strength category of the connection from equal to full-strength due to the reduced section.

Although the skeleton curves confirm that while the initial stiffness is similar across models, inelastic behaviours such as strain-hardening, moment resistance, and strength degradation slightly differ with varying web opening sizes and the presence of composite action. From the skeleton curves in Figures 10 and 11, the average difference between the sagging and hogging strengths was approximately 6%. This was due to the presence of a composite slab, leading to an asymmetric behaviour. Additionally, Figure 12 reveals that the composite slab contributes to both sagging and hogging moment capacities in all cases. The findings obtained from Figure 12 suggest a need to consider the strain hardening of material when designing RWS connections. This is because all connections achieved a minimum normalised moment above 0.98.

In this study, the effective yield (plastic) strength ratio ($M_{ye}/M_{pl,a,Rd}$) is employed to evaluate the plastic strength of a connection. The ratio $M_{ye}/M_{pl,a,Rd}$ was selected to characterise the effective yield strength of the RWS connection relative to its theoretical plastic moment capacity per Eurocode 3. Physically, $M_{ye}/M_{pl,a,Rd}$ reflects the reduction in moment capacity caused by the web openings, which localise yielding and promote a ductile response under cyclic loading. This ratio is particularly valuable, as it captures both the onset of yielding, represented by M_{ye} from experimental moment-rotation responses, and the full plastic capacity, represented by $M_{pl,a,Rd}$ from the calculated capacity according to design codes. This enables an assessment of the connection's residual strength beyond initial yield and how well the connection performs compared to design expectations. This comparison is crucial for understanding the real behaviour of RWS connections under cyclic loading conditions.

All connections (both with and without web opening) developed average strengths of 0.97 and 0.90 $M_{pl,a,Rd}$ for those with low composite action and 0.96 and 0.87 $M_{pl,a,Rd}$ for those with high composite action, respectively. All bare steel connections could achieve the nominal plastic strength of the connected beam $M_{pl,a,Rd}$. The effective yield moments (strengths) M_{ye} of bare steel connections exceeded those with composite slabs. This was expected due to the earlier yielding of the connections with composite slabs, which arises from the increased strain demand on the bottom beam flange. However, the maximum applied moments ($M_m = M_f$) of composite connections (both with low and high action) were higher than those for bare steel beams. This is attributed to the presence of the

composite slab, which increases the strength of the beam, but as aforementioned, results in an early yielding of the section.

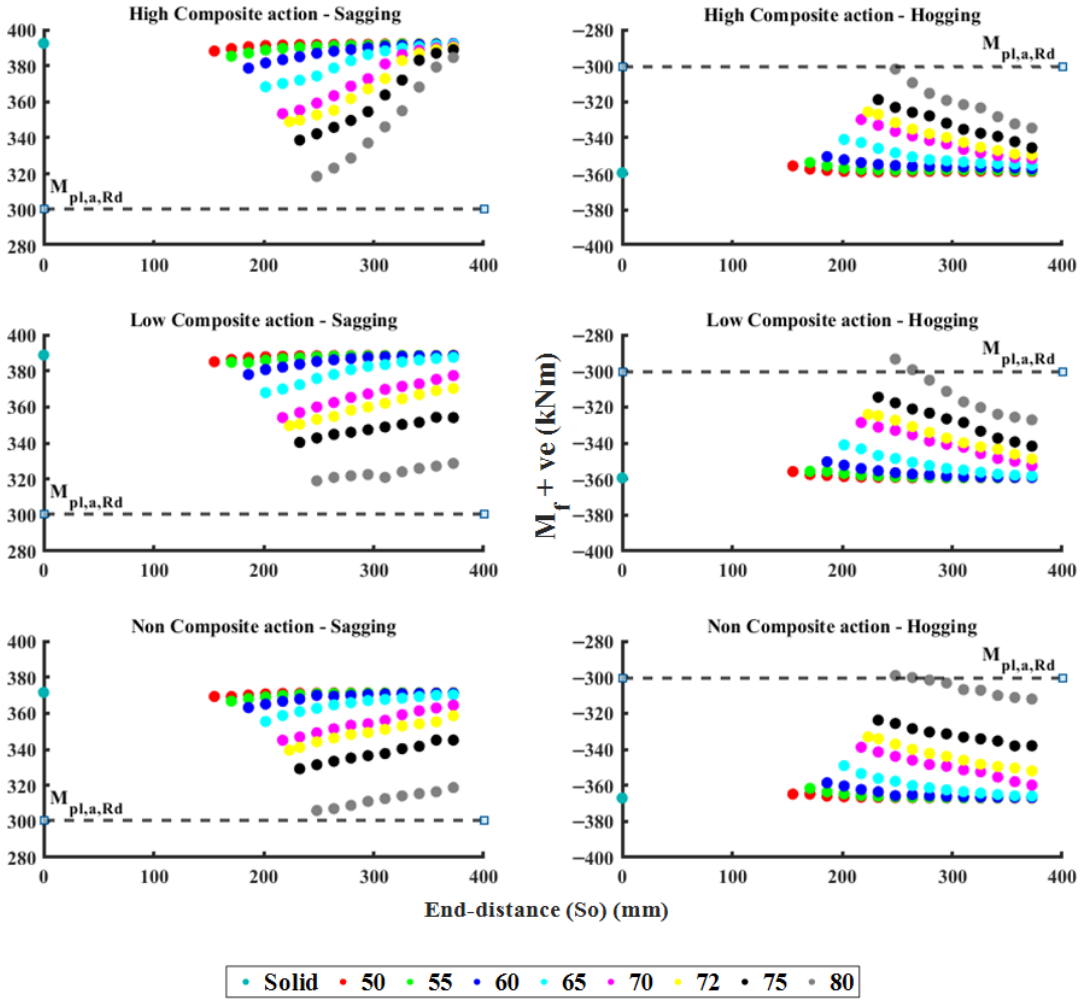

Figure 12. The effect of end-distance (S_o) on maximum applied moments at column face (M_f= M_m).

Beyond the effective yield (plastic) strength, all connections developed a maximum moment ($M_m = M_f$) of 1.23 $M_{pl,a,Rd}$ in sagging and 1.16 $M_{pl,a,Rd}$ in hogging, on average. The minimum normalised moments ($M_m/M_{pl,a,Rd}$) were 1.02 and 0.98 in sagging and hogging strengths, respectively, while the maxima for $M_m/M_{pl,a,Rd}$ were 1.31 and 1.22 in sagging and hogging strengths, respectively. This variation was highly dependent on the location and size of the web opening, as shown in Figure 12: as web opening size increases, the influence of end-distance becomes more pronounced. This can be seen in RWS connections in Set 2 (70d to 80d). This observation is consistent with previous studies of RWS connections [1–9]. An increase in end-distance resulted in a corresponding increase in both sagging and hogging moments at the column face across all composite action scenarios (high, low, and non-composite). This observation can be attributed to the greater lever arm provided by a larger end-distance, amplifying the bending moments induced by the applied loads. The presence of composite action over the protected zone generally led to slightly higher moment values than low and non-composite categories, as expected due to the increased flexural rigidity of composite action.

The applicability of Eurocode's component method for estimating the moment capacity of RWS connections was investigated. This involved comparing the moment capacity (M_{ye}) obtained from the IMK model of the RWS connections to the design moment resistance ($M_{j,Rd}$) predicted by Eurocode's component method for a bare-steel connection with a

solid webbed-beam. Although the effective yield moment (M_{ye}) is typically slightly higher than the connection's expected moment capacity ($M_{j,Rd}$) [30], the M_{ye} of the skeleton $M-\theta$ curves is a reasonable estimation of the moment capacities of RWS connections. The findings indicate that Eurocode's component method generally offers a conservative estimate of the bending resistance for RWS connections across all categories and both diameter sets (Figures 10 and 11). The observed maximum positive difference of 1.02 suggests a slight overestimation by the Eurocode method in a limited number of cases with bare-steel RWS connections. The presence of a composite slab (High and Low) appears to have minimal impact on the accuracy of the Eurocode method. This is indicated by the wider range, between 0.79 and 1.01, for all sets in both sagging and hogging. Connections without a composite slab (Non) exhibited a slightly narrower range, between 0.88 and 1.02, for all sets in both sagging and hogging. These findings suggest a close correlation between the predicted and actual resistance for RWS connections. Hence, Eurocode's component method appears to be a reliable tool for initial design estimations of the bending resistance of RWS connections.

3.2.2. Hysteretic Response

The design of all RWS connections was based on the nominal plastic bending capacity $M_{pl,a,Rd}$ of the connected steel solid-webbed beam of a partial strength connection, without considering the composite action contribution according to EC3, EC4, and EC8 [14,22,25,31]. As it was aforementioned, the strength category of the connection changed from partial to full strength due to the perforated beam. In partial strength connections, the deformations occur in the connection, leading to the pinching mechanism, which are characterised by the reduction in stiffness during reloading after unloading, along with stiffness recovery when displacement is imposed in the opposite direction [32,33]. Such a mechanism is associated with the opening and closing of gaps between the end-plate and column flange, which could result in a large reduction in the energy dissipation capacity [32,33].

The pinching mechanism occurred in all solid-webbed connections as well as in RWS connections with diameters from 0.5h, 0.55h, 0.60h, to 0.65h. Figure 13 shows that the pinching mechanism in composite RWS connections with a diameter (d_o) and end-distance (S_o) equal to 0.65h was eliminated in the last two cycles of 0.05rad. This elimination was due to the late full plastification of the perforated beam (Vierendeel mechanism), which limited the inelastic deformation in the extended end-plate. This is depicted in Figure 14, which shows the development of two plastic hinges at the low moment side (LMS). It is worth noting that the LMS is located to the right of the web opening in the cantilever setup. However, the pinching effect became more pronounced when the end-distance (S_o) increased in the composite RWS connections with diameter (d_o) equal 0.65h. All RWS connections with diameters from 0.5h, 0.55h, to 0.60h exhibited pinching behaviour, with no signs of the Vierendeel mechanism developing. In this study, all solid-webbed connections as well as RWS connections with d_o ranges from 0.5h to 0.65h did not experience strength degradation up to 0.05rad where the analysis was stopped to optimise the computational time and hard drive storage.

Ultimately, when the web opening size increases, it was observed that the pinching effects become less noticeable. As a result, the connections experience cyclic strength degradation (Figure 15). FEMA 440 [32] differentiates two types of cyclic strength degradation that a structural system might exhibit, namely cyclic degradation and in-cycle degradation [32]. The former occurs in the subsequent loading cycle due to increasing inelastic displacement, while the latter takes place within the same loading cycle because of repeated cyclic displacement. Generally, the cyclic strength degradation could lead to a stable dynamic response of a structural system [32]. In contrast, in-cycle strength degradation might

induce dynamic instability in the structural system [32]. All RWS connections studied in this paper experienced cyclic strength degradation, with reductions in strength not exceeding 20% before reaching 0.04rad. Consequently, they satisfy the seismic requirements of ANSI/AISC 358-16, ANSI/AISC 341-16 and EC8 [12,22,23].

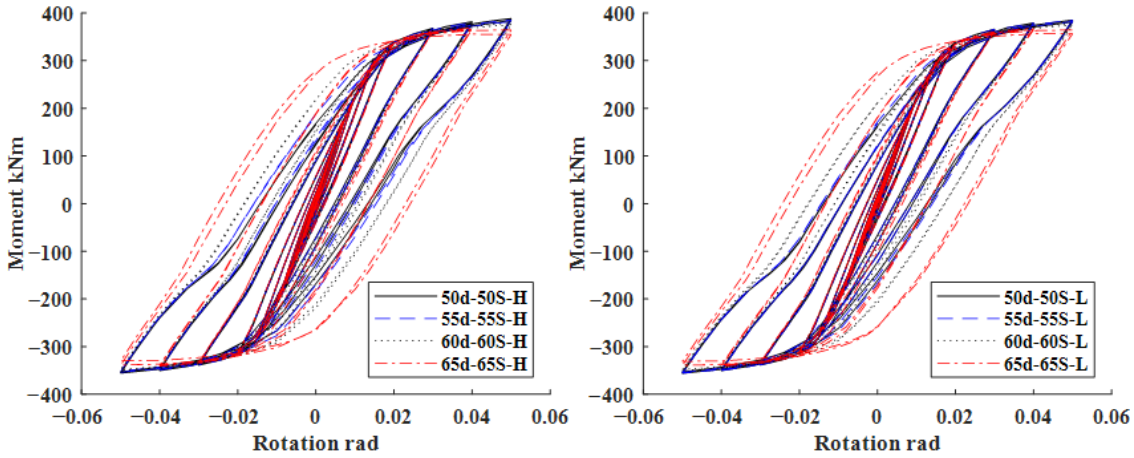

Figure 13. Moment–rotation curves for small to medium web opening with low and high composite action.

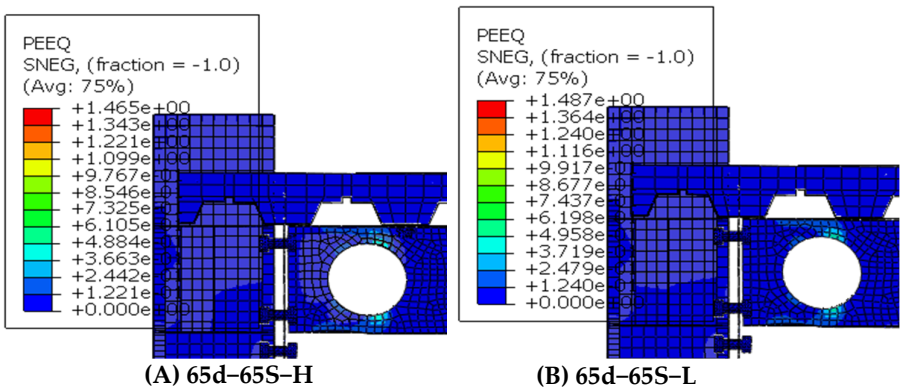

Figure 14. The development of two plastic hinges in LMS.

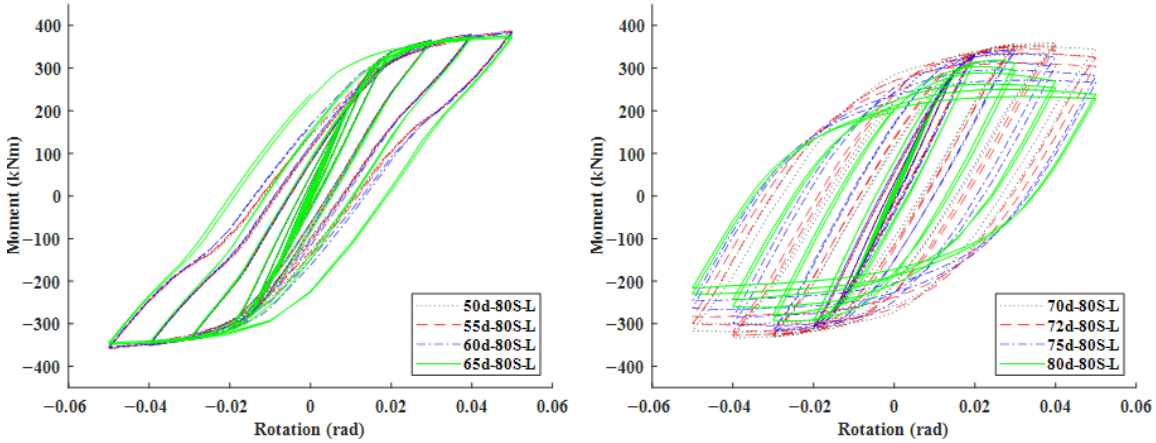

Figure 15. The effect of web opening size on the pinching mechanism.

In accordance with the findings presented by Almutairi et al. [7,8] and Shaheen et al. [9], it was found that medium to large web opening sizes were efficient in triggering the Vierendeel mechanism in composite RWS connections. This was also observed by Tsavdaridis et al. [11] and Tsavdaridis and D'Mello [34] in bare-steel RWS connections.

Herein, RWS connections with large diameters equal to 0.7h, 0.72h, 0.75h, and 0.8h were able to achieve high inelastic behaviour at the reduced section. RWS connections with diameters equal to 0.7h and 0.72h comply with SCI-P355 [10] limitations in terms of the web opening size, while the web openings with diameters equal to 0.75h and 0.8h are outside that range but are practically feasible. Both perform satisfactorily and provide an ideal structural behaviour in terms of stress distribution under cyclic loading without significantly compromising the connection capacity, provided that a suitable location for the web opening is chosen.

3.2.3. Ductility and Energy Dissipation

Aiming for reliable load transfer and redistribution within MRFs under seismic loads, ductility and energy dissipation are key characteristics. Ductility evaluates the ability of a material or structure to undergo large inelastic deformation without significant reduction in strength and is quantified as the ratio of the ultimate rotation to yield rotation (θ_u/θ_y). Energy dissipation, on the other hand, assesses the structure's capability to release seismic energy. This is achieved through the development of plastic hinges at predefined locations, which aim to minimise the force transmitted to the structure, thereby preventing accumulated damage. This attribute can be calculated by examining the area enclosed under the outer loop of the hysteresis loops at ultimate rotation. In this study, energy dissipation was calculated at a drift ratio of 0.05 rad, aligning with seismic performance expectations for RWS connections featuring a web opening diameter of 0.8h and end-distance of 0.8h. This configuration exceeds the limitations set by the SCI-P355 guidance and is validated by recent experimental tests conducted by Almutairi et al. [8]. These drift ratios enable us to capture energy release across the structural response under varying levels of cyclic loading.

Figures 16 and 17 illustrate the effect of the web opening size on both ductility and energy dissipation, respectively. RWS connections with high composite action exhibit the highest ductility ratios as a result of early initiation of yielding due to the high strain demand on the beam's bottom flange. Also, this high strain demand leads to greater ductility under hogging moment in RWS connections with high composite action. The difference between RWS connections with high and low composite action is approximately 4% and 5%, on average under sagging and hogging moments, respectively. The outlier in the RWS connections is with a diameter equal to 0.75h, due to an early termination of the analysis at 0.04rad under a hogging moment. The analysis was terminated early due to exceeding the allotted time on the high-performance computer. However, this should not distort the observation that as the web opening size increases, the ductility also increases. Conversely, ductility decreases as the web opening location is located away (i.e., as end-distance increases). Non-composite RWS connections display lower ductility ratios due to their relatively high yield rotations.

Regarding energy dissipation, RWS connections with low composite action exhibit the highest values when the diameter ranges from 0.72h to 0.8h among all connections. For diameters ranging from 0.5h to 0.7h, connections with high composite action dissipate more energy than their counterparts with low composite action. This observation is also consistent for connections with solid-webbed beams. For connections with non-composite beams, the dissipated energy increases as the web opening size increases. As observed with the ductility predictions, the dissipated energy decreases as the location of the web opening moves further away, or in other words, as the end-post (end distance) increases. Among all connection models, the solid-webbed beam connection demonstrated the lowest energy dissipation values. Under the specific design parameters examined, incorporating web openings has shown potential for increased energy dissipation due to plastification

at the reduced section via the Vierendeel. Thus, the findings presented here are primarily applicable within the specific design conditions studied.

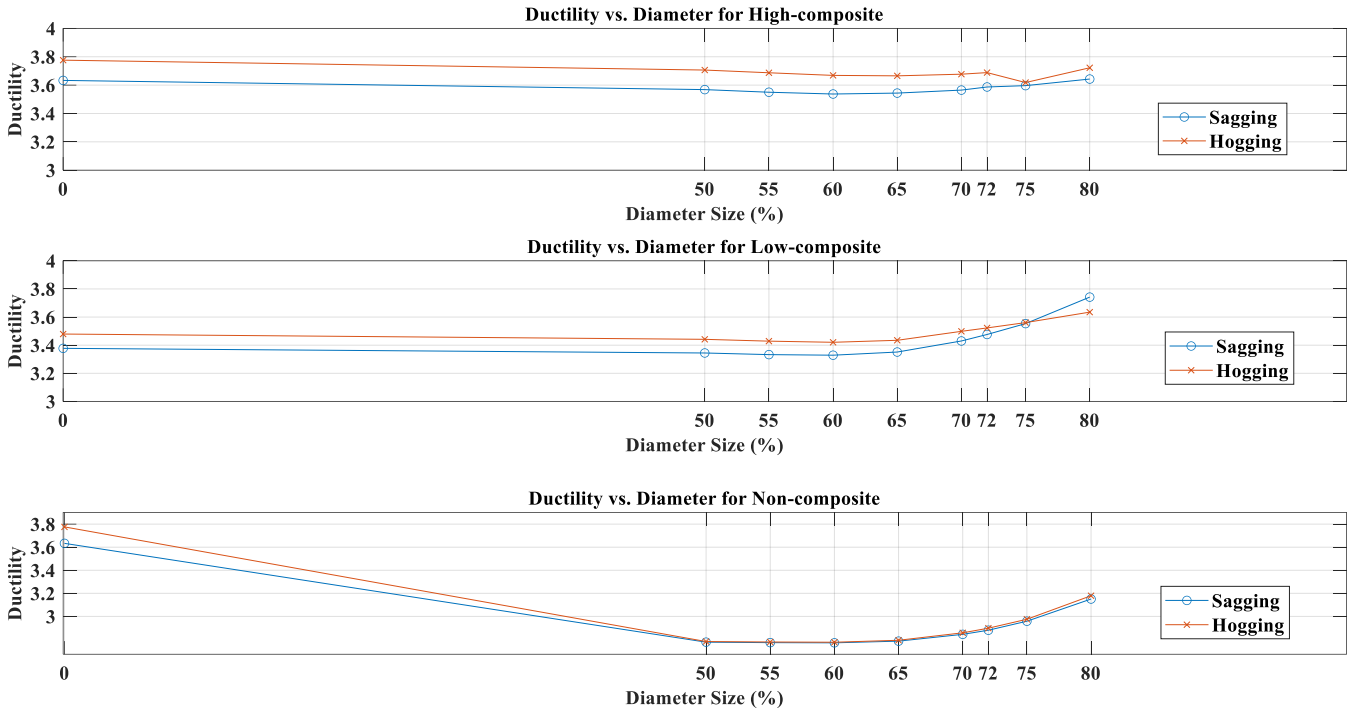

Figure 16. The trend of the ductility vs. diameter (on average).

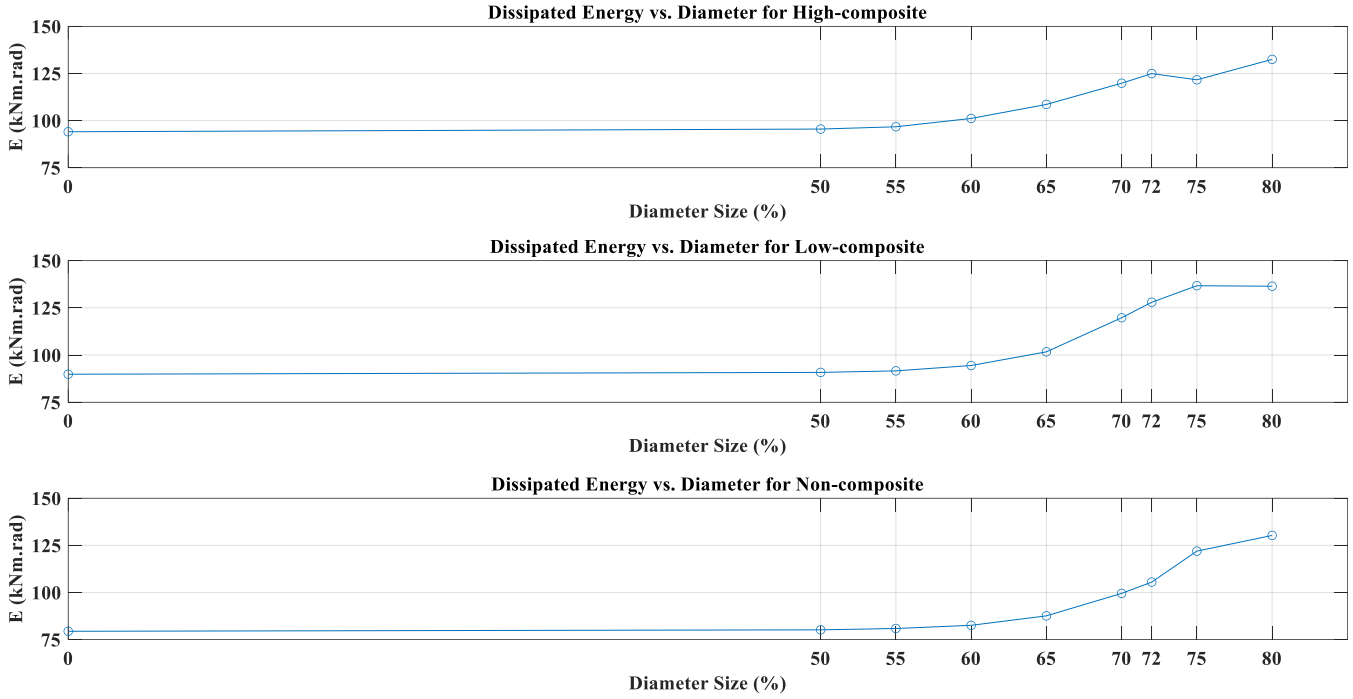

Figure 17. The trend of the dissipated energy vs. diameter (on average).

3.2.4. Contribution of the Composite Metal Deck Slab

Figure 18 illustrates the composite slab's contribution to connection strength under sagging moments, contrasting with negligible effects under hogging moments. The composite beam induces an asymmetric cyclic response—unlike the symmetric behaviour of bare steel connections—because the slab engages the beam's top section in sagging, while only

the steel section resists hogging. This asymmetry highlights the slab's role in enhancing sagging capacity, a critical consideration for seismic design.

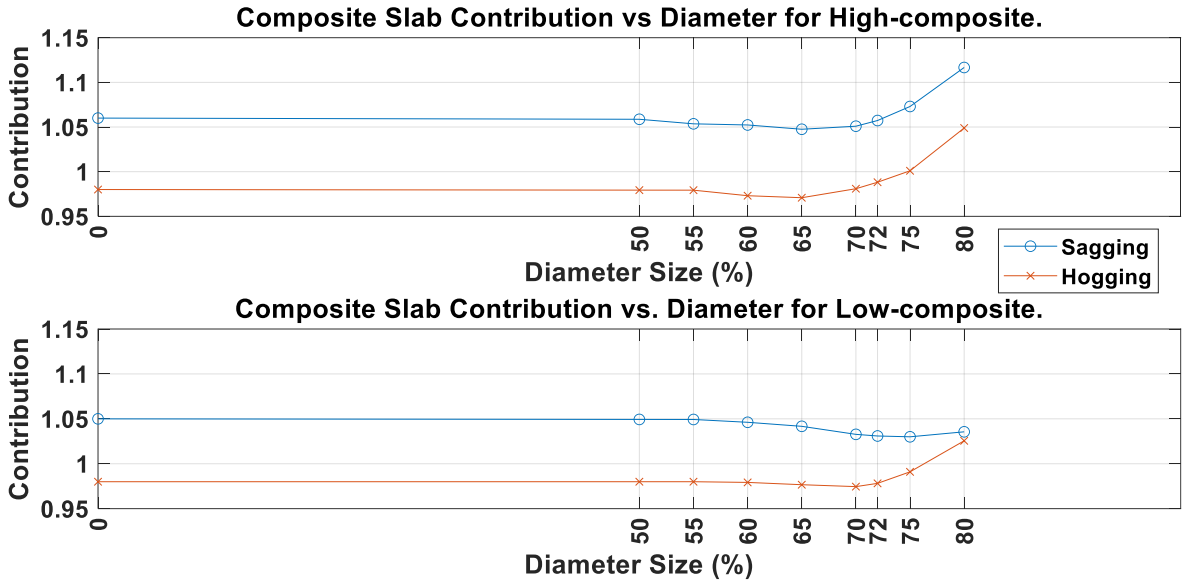

Figure 18. Contribution of RC slab to maximum strength of the connections (on average); $M_{m,comp}$ and $M_{m,non-comp}$, refer to maximum moment for composite and non-composite counterpart.

Despite this, the maximum strengths of the connections were slightly similar between the RWS connections with and without bolted studs over the web opening (protected zone) for most diameters (i.e., 0.5h to 0.7h). This similarity can be attributed to the elimination of contact between the concrete slabs and the extended end-plates and columns (i.e., 25 mm gap) in all connections. This 25 mm gap restricts the force transfer from the composite slab to the extended end-plates and columns. Consequently, the additional row of bolted shear studs provided in the RWS connections with high composite action does not affect the overall strength of the connection, although it does have an impact on ductility, in which the presence of composite action leads to the early yielding.

For RWS connections with diameters ranging from 0.72h to 0.8h, the contribution of the composite slab increases in both sagging and hogging moments. With RWS connections of diameter equal to 0.8h, the composite slab contributes, on average, 5% to the overall strength. It is also observed that as the web opening moved further away, the contribution of the composite slab increases. This observation aligns with previous studies of composite RWS connections [7,9]. These findings suggest that, in general, when using bolted shear studs, the strength of the composite connection is easier to predict than with the traditional welded shear studs, which could contribute up to a 60% [7,9]. Another key observation is that the level of damage (in the form of cracking and crushing) remained minimal, largely because of the oversized holes for bolted shear studs.

3.3. Applicability of SCI-P355 Guidance

The hysteretic behaviour of bolted extended end-plate RWS connections with demountable composite metal deck slabs can arise from complex deformations that span multiple connection components (e.g., web opening, end-plate, bolts, etc.). Given the range of components that may undergo deformation in elastic and plastic regions, predicting the hysteresis behaviour of such connections could be challenging. In the literature, there is no consensus on computing the moment capacity of RWS connections ($M_{RWS,Rd}$).

In this study, the IMK model is employed to determine the effective yield moment (M_{ye}) representing the moment capacity of RWS connections. This approach is followed

as the design guidance in Eurocode 3 [14] and SCI-P355 [10] rely on the nominal (or measured) yield strength (f_y) to compute the expected capacity of a member. The expected plastic bending capacity of a steel beam is typically defined based on the nominal (or measured) yield strength (f_y) multiplied by the plastic section modulus of the major axis (Z) in accordance with Eurocode 3 [14]. In addition, the bending of the beam at the opening ($M_{o,Rd}$), as per SCI-P355 guidance [10] (excluding the composite slab contribution), is determined as the product of the following:

i. Area of the two Tee sections ($A_{T,e,o}$);
ii. Yield strength (f_y); and,
iii. Effective depth between the centroid of the Tees (h_{eff}).

The difference between the maximum moment M_m and the effective yield moment (M_{ye}) can be considered as the additional strength possessed by the connection due to strain-hardening and second-order effects that develop, resulting from deformations across multiple connection components.

The effective yield moments (M_{ye}) obtained from the skeleton $M-\theta$ curves are compared with the bending of the beam at opening ($M_{o,Rd}$) in accordance with SCI-P355 guidance [10]. The outcomes indicate that the $M_{ye}/M_{o,Rd}$ have an average (μ), standard deviation (σ), minimum (min), and maximum (max) of 1.06, 0.05, 0.95 and 1.13 under sagging moment, respectively. The ratio of $M_{ye}/M_{o,Rd}$ under hogging moment has μ, σ, min and max values of -1, 0.05, -0.89 and -1.1, respectively. A general tendency is detected, and SCI-P355 guidance could predict the moment strength of bolted extended end-plate RWS connections with demountable composite slab under cyclic loads. The findings show an acceptable strain-hardening ratio M_m/M_{ye} of 1.26, on average. Table 3 displays the average (μ), standard deviation (σ), minimum (min), and maximum (max) values for different sets of diameters.

Table 3. Statistics for different sets of diameters based on the ratio of $M_{ye}/M_{o,Rd}$.

Diameter d_o	Composite (H/L)/ Non-Composite	Average μ		Max		Min		Standard Deviation σ	
		+ve	−ve	+ve	−ve	+ve	−ve	+ve	−ve
50	High	1.02	−0.93	1.02	1.00	−0.91	−0.93	0.01	0.01
	Low	1.05	−0.96	1.05	1.04	−0.95	−0.97	0.00	0.00
	Non-comp	1.06	−1.05	1.07	1.06	−1.05	−1.06	0.00	0.00
55	High	1.03	−0.94	1.04	1.01	−0.92	−0.95	0.01	0.01
	Low	1.06	−0.97	1.07	1.05	−0.96	−0.98	0.01	0.01
	Non-comp	1.07	−1.06	1.08	1.07	−1.06	−1.07	0.00	0.00
60	High	1.04	−0.95	1.06	1.01	−0.93	−0.96	0.02	0.01
	Low	1.07	−0.98	1.08	1.05	−0.96	−0.99	0.01	0.01
	Non-comp	1.09	−1.07	1.09	1.07	−1.06	−1.08	0.01	0.01
65	High	1.05	−0.96	1.07	1.00	−0.93	−0.97	0.03	0.02
	Low	1.07	−0.99	1.09	1.04	−0.96	−1.00	0.02	0.02
	Non-comp	1.09	−1.08	1.10	1.08	−1.06	−1.09	0.01	0.01
70	High	1.05	−0.96	1.09	0.99	−0.92	−0.98	0.04	0.02
	Low	1.06	−0.98	1.09	1.03	−0.95	−1.01	0.02	0.02
	Non-comp	1.09	−1.08	1.11	1.07	−1.06	−1.10	0.01	0.01

Table 3. *Cont.*

Diameter d_o	Composite (H/L)/ Non-Composite	Average μ		Max		Min		Standard Deviation σ	
		+ve	−ve	+ve	−ve	+ve	−ve	+ve	−ve
72	High	1.05	−0.96	1.10	0.98	−0.92	−0.98	0.05	0.02
	Low	1.05	−0.98	1.08	1.02	−0.95	−1.01	0.02	0.02
	Non-comp	1.09	−1.07	1.10	1.07	−1.05	−1.09	0.01	0.01
75	High	1.05	−0.96	1.12	0.97	−0.92	−0.99	0.05	0.02
	Low	1.04	−0.97	1.06	1.01	−0.93	−1.00	0.02	0.02
	Non-comp	1.07	−1.06	1.09	1.06	−1.04	−1.07	0.01	0.01
80	High	1.04	−0.95	1.13	0.95	−0.90	−0.98	0.07	0.03
	Low	1.00	−0.95	1.02	0.97	−0.89	−0.99	0.01	0.03
	Non-comp	1.04	−1.02	1.05	1.02	−1.00	−1.03	0.01	0.01

3.4. Capacity Design Ratio

All RWS connections were designed based on the connected steel solid-webbed beam section strength $M_{pl,a,Rd}$, of a partial/equal-strength connection, without considering the contribution of the composite action according to EC3, EC4, and EC8, aiming for the introduction of a web opening to alter the strength category of the connection from partial to full strength due to the reduction in the strength of the connected steel beam section. However, there is no consensus in the literature on the extent of reductions in strength that arise due to the size and location of the web opening.

Knowing the amount of reduction in the moment capacity of the connected beam will change the capacity design ratio of the column/connection to the connected steel–concrete composite beam. This is significant when retrofitting existing buildings to optimise the resources in choosing the optimum size and location of the web opening to achieve the required capacity design ratio. Many studies have demonstrated the ability of a large web opening in the high shear zone to develop a ductile (Vierendeel) mechanism [1–9]. However, this is not always the case, as Shaheen et al. [9] previously concluded that small-to-medium web opening sizes should be considered instead owing to the negative impact of large web openings on the cyclic behaviour of composite RWS connections. The findings of the recent experimental and FE studies by Almutairi et al. [7,8] highlighted the importance of the capacity design ratio in the design of RWS connections. Consequently, understanding the capacity design ratio as well as the composite action effects on the seismic performance of the RWS connections is critical for both new and existing buildings.

Figures 19 and 20 present a comparison between a full-strength connection and an equal/partial-strength connection. Both connections are identical in terms of the presence of composite action over the protected zone, as well as the size and material of steel and concrete sections. The only difference lies in the thickness of the end-plates; the full-strength connection has a thickness of 30 mm, while the equal-/partial-strength connection has a thickness of 20 mm. This resulted in a 6% increase in the capacity of the connection. The comparison was conducted employing small-to-medium diameters of web openings (0.5h, 0.55h, and 0.65h). The pinching phenomenon occurred in both types of solid-webbed connections. In the partial/equal-strength connection, the extended end-plate is the main source of plastic deformation; hence, the pinching effect is more pronounced than in the full strength connection. As the diameter increases, the pinching effects diminish, especially in the full-strength connection. This is consistent with the findings of Almutairi et al. [7], which proved the efficiency of introducing a web opening to alter the strength category and make the reduced section in the beam the main element to dissipate energy by developing

plasticity. The results confirm the findings of Shaheen et al. [9] regarding small-to-medium web opening sizes, as the high capacity design ratio was provided in [9]. It can be concluded that when a high-capacity design ratio is provided, low to medium web opening sizes should be used, and vice versa. It is worth noting that large diameters have not been used in this comparison, as their efficiency in triggering the Vierendeel mechanism has been established, provided that the proper location is chosen.

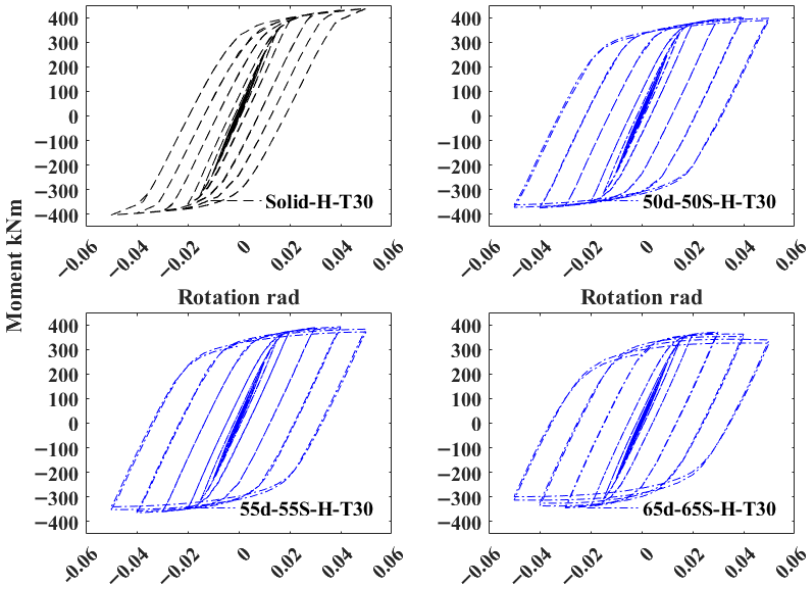

Figure 19. Full-strength connection—thickness of end-plate = 30 mm $M_{j,Rd}/M_{\mathrm{pl,a,R}}$ = 1.06.

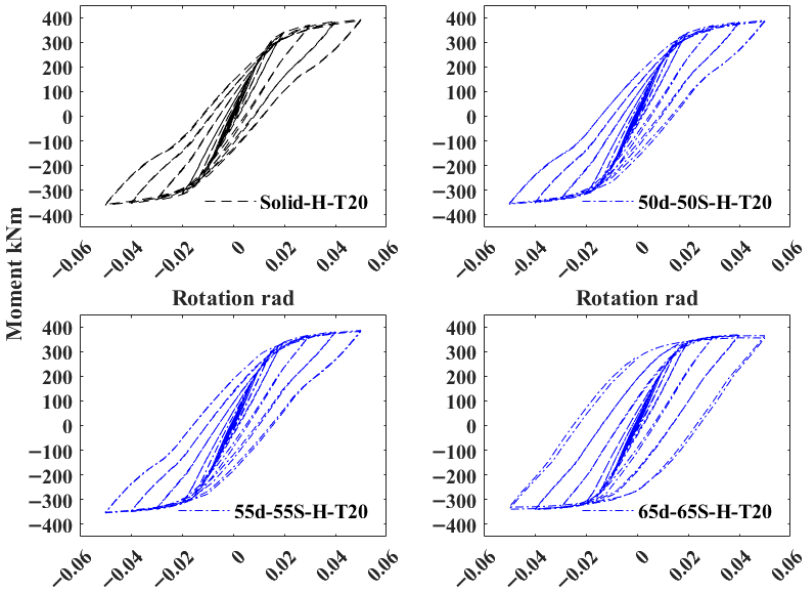

Figure 20. Equal/partial-strength connection—thickness of end-plate = 20 mm $M_{j,Rd}/M_{\mathrm{pl,a,R}}$ = 1 with high composite action in terms of capacity ratio.

4. Concluding Remarks

The hysteretic response characteristics of demountable extended end-plate bolter steel–concrete composite connections with reduced web section (RWS) have been quantified and assessed followed by an experimental study in this paper for the first time. The assessment is based on a parametric high-fidelity FEA database that comprises 285 models. The parametric results are employed to gain a better understanding of the local cyclic behaviours of composite RWS connections. Response parameters derived from skeleton

M-θ relationships using the IMK model were evaluated. These parameters include stiffness, strength, and ductility. Moreover, the contribution of the composite metal deck slab to the overall strength of the RWS connection was investigated by comparing the composite RWS connections to their RWS steel counterparts. Both the bending moment $M_{o,Rd}$ and Vierendeel bending $M_{v,Rd}$ capacities are also assessed in accordance with SCI-P355 guidance [10]. The following conclusions are drawn from this study:

- As the web opening size increases, the pinching effect diminishes.
- Ductility increases with the increase in the size of the web opening but decreases as the end distance increases.
- RWS connections effectively enhance energy dissipation through the plastification of the perforated section.
- RWS connections with diameters from $0.7h$ to $0.8h$ efficiently triggered the Vierendeel mechanism under cyclic loads. For such composite RWS connections, the ductility and energy dissipation increase up to 13% and 57%, respectively, with a reduction in capacity up to 19%, compared to a solid-webbed connection.
- When an equal capacity design ratio between the connection and beam was used,
    - For RWS connections with the presence of composite action, the ideal d_o/S_o ratio is equal to 1.0.
    - For RWS connections with the absence of composite action, d_o/S_o ratio between 0.8 and 1.0 is recommended, provided that the end-post distance adheres to the requirements specified in SCI P355 guidance.
- The presence of bolted shear studs over the protected zone influences ductility, potentially leading to early yielding of the perforated section.
- Bolted shear studs provide more consistent and predictable strength compared to traditional welded shear studs, contributing approximately 5% to the connection's strength.
- SCI P355 guidance can be employed to estimate the bending moment at the opening of RWS connections with demountable composite slabs under cyclic loads.

Limitations of this study include the validation of the FE models against four experimental specimens, the use of a fixed beam size throughout the parametric investigation, and the focus on local behaviour rather than the global MRF response, which may limit the general applicability of the findings. Future work should address these limitations by expanding experimental validation across different connection configurations and loading protocols, analysing multi-storey MRFs to understand global structural implications, refining Vierendeel capacity predictions with additional experimental data, and investigating varied material properties and dynamic loading protocols. Such extensions would strengthen design recommendations and broaden applicability.

Author Contributions: Conceptualization, F.F.A. and K.D.T.; methodology, F.F.A. and K.D.T.; software, F.F.A.; validation, F.F.A.; formal analysis, F.F.A. and K.D.T.; investigation, F.F.A. and K.D.T.; resources, F.F.A. and K.D.T.; data curation, F.F.A.; writing—original draft preparation, F.F.A. and K.D.T.; writing—review and editing, F.F.A. and K.D.T.; visualization, F.F.A.; supervision, K.D.T. All authors have read and agreed to the published version of the manuscript.

Funding: This research received no external funding.

Data Availability Statement: The database is publicly available in a Mendeley (2020) data repository (https://doi.org/10.17632/8hk4dbzks4.1).

Conflicts of Interest: The authors declare no conflicts of interest.

References

1. Yang, Q.; Li, B.; Yang, N. Aseismic behaviors of steel moment resisting frames with opening in beam web. *J. Constr. Steel Res.* **2009**, *65*, 1323–1336. [CrossRef]
2. Zhang, X.; Zheng, S.; Zhao, X. Seismic performance of steel beam-to-column moment connections with different structural forms. *J. Constr. Steel Res.* **2019**, *158*, 130–142. [CrossRef]
3. Tsavdaridis, K.D.; Papadopoulos, T. A FE parametric study of RWS beam-to-column bolted connections with cellular beams. *J. Constr. Steel Res.* **2016**, *116*, 92–113. [CrossRef]
4. Boushehri, K.; Tsavdaridis, K.D.; Cai, G. Seismic behaviour of RWS moment connections to deep columns with European sections. *J. Constr. Steel Res.* **2019**, *161*, 416–435. [CrossRef]
5. Tsavdaridis, K.D.; Lau, C.K.; Alonso-Rodríguez, A. Experimental behaviour of non-seismical RWS connections with perforated beams under cyclic actions. *J. Constr. Steel Res.* **2021**, *183*, 106756. [CrossRef]
6. Tabar, A.M.; Alonso-Rodriguez, A.; Daniel Tsavdaridis, K. Building Retrofit with Reduced Web (RWS) and Beam (RBS) Section Limited-Ductility Connections. *J. Constr. Steel Res.* **2022**, *197*, 107459. [CrossRef]
7. Almutairi, F.F.; Tsavdaridis, K.D.; Alonso Rodriguez, A.; Asteris, P.G.; Lemonis, M.E. Hysteretic Behaviour of Composite Reduced Web Section (RWS) Connections for Seismic Applications. *J. Earthq. Eng.* **2023**, *28*, 349–384. [CrossRef]
8. Almutairi, F.F.; Tsavdaridis, K.D.; Alonso-Rodriguez, A.; Hajirasouliha, I. Experimental investigation using demountable steel-concrete composite reduced web section (RWS) connections under cyclic loads. *Bull. Earthq. Eng.* **2024**, *22*, 1081–1110. [CrossRef]
9. Shaheen, M.A.; Tsavdaridis, K.D.; Yamada, S. Comprehensive FE Study of the Hysteretic Behaviour of Steel-Concrete Composite and Non-Composite RWS Beam-to-Column Connections. *J. Struct. Eng.* **2018**, *144*, 04018150. [CrossRef]
10. Lawson, R.M.; Hicks, S.J. *Design of Composite Beams with Large Web Openings*; SCI Publication: Berkshire, UK, 2011.
11. Tsavdaridis, K.D.; Pilbin, C.; Lau, C.K. FE parametric study of RWS/WUF-B moment connections with elliptically-based beam web openings under monotonic and cyclic loading. *Int. J. Steel Struct.* **2017**, *17*, 677–694. [CrossRef]
12. *ANSI/AISC 341-16*; Seismic Provisions for Structural Steel Buildings. American Institute of Steel Construction, AISC: Chicago, IL, USA, 2016; p. 60601.
13. Tsavdaridis, K.D.; D'Mello, C. FE investigation of perforated sections with standard and non-standard web opening configurations and sizes. In *Proceedings of the 6th International Conference on Advances Is Steel Structures*; Hong Kong Institute of Steel Construction: Hong Kong, China, 2009.
14. European Committee for Standardization. *CEN Eurocode 3: Design of Steel Structures—Part 1-1: General Rules and Rules for Buildings*; European Committee for Standardization: Brussels, Belgium, 2005.
15. *ABAQUS Abaqus User's Manual*, Version 6.19; Dassault Systèmes Simulia: Johnston, RI, USA, 2019.
16. Hosseini, S.M.; Rahnavard, R. Numerical study of steel rigid collar connection affecting cyclic loading. *Eng. Struct.* **2020**, *208*, 110314. [CrossRef]
17. Almutairi, F.F.; Tsavdaridis, K.D. Capacity design assessment of composite reduced web section (RWS) connections. *Eng. Struct.* **2024**, *316*, 118558. [CrossRef]
18. European Committee for Standardization. *CEN Eurocode 2: Design of Concrete Structures—Part 1.1: General Rules and Rules for Buildings*; European Committee for Standardization: Brussels, Belgium, 2004.
19. Cornelissen, H.A.W.; Hordijk, D.A.; Reinhardt, H. Experimental determination of crack softening characteristics of normalweight and lightweight. *Heron* **1986**, *31*, 45–56.
20. Qureshi, J.; Lam, D.; Ye, J. Finite element modelling of shear connection behaviour in a push test using profiled sheeting. In *Advances and Trends in Structural Engineering, Mechanics and Computation*; CRC: Boca Raton, FL, USA, 2010; p. 167.
21. Ahmed, I.M.; Tsavdaridis, K.D. Shear connection of prefabricated ultra-lightweight concrete slab systems (PUSSTM). In *Proceedings of the Structures*; Elsevier: Amsterdam, The Netherlands, 2022; Volume 36, pp. 65–97.
22. European Committee for Standardization. *CEN Eurocode 8: Design of Structures for Earthquake Resistance—Part 1: General Rules, Seismic Actions and Rules for Buildings*; BSI: London, UK, 2005.
23. *ANSI/AISC 358-16*; Prequalified Connections for Special and Intermediate Steel Moment Frames for Seismic Applications. AISC: Chicago, IL, USA, 2016.
24. Ibarra, L.F.; Medina, R.A.; Krawinkler, H. Hysteretic models that incorporate strength and stiffness deterioration. *Earthq. Eng. Struct. Dyn.* **2005**, *34*, 1489–1511. [CrossRef]
25. *EN 1993-1-8: 2005*; CEN Eurocode 3: Design of Steel Structures—Part 1–8: Design of Joints. European Committee for Standardization: Brussels, Belgium, 2005.
26. Ding, Z.; Elkady, A. Semirigid Bolted Endplate Moment Connections: Review and Experimental-Based Assessment of Available Predictive Models. *J. Struct. Eng.* **2023**, *149*, 4023117. [CrossRef]
27. D'Aniello, M.; Tartaglia, R.; Landolfo, R.; Jaspart, J.-P.; Demonceau, J.-F. Seismic pre-qualification tests of EC8-compliant external extended stiffened end-plate beam-to-column joints. *Eng. Struct.* **2023**, *291*, 116386. [CrossRef]

28. Landolfo, R. European seismic prequalification of steel beam-to-column joints: EQUALJOINTS and EQUALJOINTS-Plus projects. *J. Constr. Steel Res.* **2022**, *192*, 107238. [CrossRef]
29. Tartaglia, R.; D'Aniello, M.; Landolfo, R. Seismic performance of Eurocode-compliant ductile steel MRFs. *Earthq. Eng. Struct. Dyn.* **2022**, *51*, 2527–2552. [CrossRef]
30. Lignos, D.G.; Krawinkler, H. Deterioration modeling of steel components in support of collapse prediction of steel moment frames under earthquake loading. *J. Struct. Eng.* **2011**, *137*, 1291–1302. [CrossRef]
31. European Committee for Standardization. *CEN Eurocode 4. Design of Composite Steel and Concrete Structures—Part 1.1: General Rules and Rules for Buildings*; BSI: London, UK, 2005.
32. Federal Emergency Management Agency (FEMA). *Effects of Strength and Stiffness Degradation on Seismic Response*; FEMA P440A; FEMA: Washington, DC, USA, 2009.
33. D'Aniello, M.; Tartaglia, R.; Costanzo, S.; Landolfo, R. Seismic design of extended stiffened end-plate joints in the framework of Eurocodes. *J. Constr. Steel Res.* **2017**, *128*, 512–527. [CrossRef]
34. Tsavdaridis, K.D.; D'Mello, C. Vierendeel bending study of perforated steel beams with various novel web opening shapes through nonlinear finite-element analyses. *J. Struct. Eng.* **2012**, *138*, 1214–1230. [CrossRef]